https://doi.org/10.5194/egusphere-2026-4588
Preprint. Discussion started: 21 August 2026

ALERT: A Scalable Cloud-Native Framework for Satellite Rainfall-Driven Landslide Early Warning in Data-Scarce Regions

Ali P. Yunus[1*], Erakkath Faizah[1], Saju Mukundan[1], Kochappi Sathyan Sajinkumar[2], Srikrishnan Siva Subramanian[3], Raju Attada[1] and Ashokan Laila Achu[1]
[1]Department of Earth and Environmental Sciences, Indian Institute of Science Education and Research Mohali, Mohali 140306, India.
[2]Department of Geology, University of Kerala, Thiruvananthapuram 695581, India
[3]Centre of Excellence in Disaster Mitigation and Management, Indian Institute of Technology Roorkee, Roorkee, Uttarakhand 247667, India.
Correspondence to: Ali P. Yunus (yunusp@iisermohali.ac.in)

Abstract. Rainfall-triggered landslides cause thousands of fatalities each year, yet effective early warning remains challenging across many mountainous regions because of sparse rainfall observations and limited forecasting infrastructure. Here we present ALERT (Automated Landslide Early Risk Tracker), a scalable, cloud-native framework that integrates NASA IMERG satellite precipitation, ECMWF operational forecasts, terrain susceptibility, rainfall intensity–duration thresholds, debris-flow runout modelling, and building exposure to deliver near-real-time, impact-based landslide warnings. ALERT incorporates a globally transferable catalogue of 24 rainfall thresholds while allowing user-defined thresholds and susceptibility layers, enabling deployment across diverse climatic and geomorphological settings. Event-based validation achieved a sensitivity of 0.80 and an overall accuracy exceeding 0.70, demonstrating effective detection of hazardous rainfall conditions for landslide initiation. By reducing dependence on dense ground-based rain-gauge networks, ALERT provides a computationally efficient and scalable pathway towards regional scale landslide early warning and climate-resilient disaster risk reduction, particularly in data-scarce regions.

1 Introduction

Landslides are among the most destructive geomorphic hazards globally, responsible for thousands of fatalities and billions of dollars in economic losses annually (Fidan et al., 2026; Froude & Petley, 2018). In tropical and subtropical mountainous regions, rainfall-triggered landslides are particularly prevalent due to the deeply weathered regolith, intense monsoonal precipitation, and high population exposure (Abraham et al. 2019; Kaushal et al. 2025). The convergence of natural susceptibility and societal vulnerability is especially severe in tectonically active and climatically dynamic mountain belts across South Asia, Southeast Asia, Central America, and sub-Saharan Africa, where rapid land-use change further amplifies instability risk (Froude & Petley, 2018; Merghadi et al., 2020).

Despite the recognized severity of the landslide hazards across these regions, operational early warning systems remain largely underdeveloped. Developing an early warning system requires the identification of threshold conditions typically expressed in terms of rainfall intensity, duration, or antecedent soil moisture, beyond which slope failure becomes more likely. Rainfall

https://doi.org/10.5194/egusphere-2026-4588
Preprint. Discussion started: 21 August 2026

intensity–duration (ID) thresholds are among the most widely adopted approaches for forecasting potential landslide occurrence (Gonzalez et al., 2024; Guzzetti et al., 2007; Osanai et al., 2010). However, rain-gauge networks in many landslide-prone regions are sparse and unevenly distributed, while systematic landslide inventories are often limited in spatial extent, temporal coverage, and reporting consistency (Abraham et al., 2020). These observational gaps compound the inherent challenges of landslide prediction, including the nonlinear interactions among rainfall, subsurface hydrology, soil properties, and slope geometry that govern slope instability (Yunus et al., 2021).

Satellite remote sensing offers a compelling pathway to overcome these observational limitations. Spaceborne precipitation products, particularly NASA's Integrated Multi-satellitE Retrievals for GPM (IMERG), provide near-global, sub-daily rainfall estimates at a spatial resolution of 0.1° and a temporal resolution of 30 min, enabling the derivation and application of rainfall intensity–duration (ID) thresholds for landslide initiation in regions lacking dense ground-based observations (Wang et al., 2023; Zhao et al., 2022). Complementing these observations, the European Centre for Medium-Range Weather Forecasts (ECMWF) Integrated Forecasting System (IFS) provides numerical weather prediction with lead times of up to 15 days, enabling a transition from near-real-time rainfall monitoring to forecast-based rainfall accumulation. Similarly, satellite-derived topographic, vegetation, and land-cover datasets support the construction of spatially continuous susceptibility maps using machine-learning approaches (Chang et al., 2019; Dou et al., 2020; Merghadi et al., 2020). In addition, cloud-computing platforms such as Google Earth Engine (GEE) facilitate the processing of large, multi-source Earth observation datasets at planetary scale, reducing the computational barriers to operational integration of these products in data-scarce environments (Laghari et al., 2025).

Critically, this convergence of satellite-based observations and cloud-scale computation creates a tractable pathway for deriving and operationalizing physically informed rainfall thresholds at regional scales where ground-based monitoring networks remain inadequate. Empirical ID thresholds, formalized by Caine, (1980), and subsequently, refined by numerous researchers (Guzzetti et al., 2007; Peruccacci et al., 2012), remain among the most widely applied approaches for operational rainfall-based landslide warning. The power-law relationship

$$I = \alpha.D^{\beta} \quad (\beta < 0)$$

where (I) is rainfall intensity (mm h^{-1}), and (D) is event duration (h), and the equation defines the lower bound of rainfall conditions associated with observed landslides. Regional calibration of the parameters α and β using satellite rainfall records and a multi-year landslide inventory is therefore a scientifically justified and computationally feasible approach for data-scarce regions (Jiang et al., 2022; Niyokwiringirwa et al., 2024). While considerable progress has been made in regional and global

https://doi.org/10.5194/egusphere-2026-4588
Preprint. Discussion started: 21 August 2026

threshold derivation (Guzzetti et al. 2007; 2025), systematic calibration at the regional scale where terrain, climate, and soil conditions vary substantially, has received comparatively limited attention.

Here, we present ALERT (Automated Landslide Early Risk Tracker), a cloud-native, scalable landslide early warning framework designed for operational deployment across data-scarce mountain environments. ALERT integrates: (i) satellite-derived rainfall thresholds calibrated from IMERG precipitation; (ii) globally transferable regional threshold parameterization; (iii) susceptibility-constrained rainfall exceedance mapping; (iv) near-real-time hindcast capability using IMERG and forecasting using ECMWF operational products; and (v) empirical runout and building exposure modelling within a unified architecture.

To evaluate the framework, we use the Western Ghats of India as a primary calibration and validation domain due to its high rainfall variability, recurrent catastrophic landslides, and extensive multi-year inventory availability. However, unlike conventional regional early warning studies, the ALERT architecture is explicitly designed for large-scale deployment through threshold interoperability and globally accessible Earth observation datasets. The framework therefore represents a scalable pathway toward operational landslide early warning in ungauged and infrastructure-limited mountain systems in diverse regions.

2 Operational Landslide Early Warning Systems – Current Status

Most operational landslide early warning systems (LEWS) currently function at regional or national scales using dense ground-based rainfall monitoring networks. Italy operates one of the most mature national systems through the Italian Civil Protection Department, which integrates weather radar observations with regional susceptibility information to issue rainfall-induced landslide warnings. Similarly, the Japan Meteorological Agency employs a nationwide warning framework based on cumulative rainfall and a Soil Water Index derived from weather radar observations to provide operational debris-flow and shallow landslide warnings (Osanai et al., 2010; Ariyakumara & Uchida 2026). Norway's national warning service, managed by the Norwegian Water Resources and Energy Directorate, combines meteorological forecasts with hydrological modelling to predict landslide-prone conditions (Devoli et al., 2018). At the municipal scale, Rio de Janeiro's Alerta Rio system integrates rainfall thresholds from numerous rain gauges with susceptibility maps to support evacuation decisions, while the United States Geological Survey maintains site-specific monitoring systems using rain gauges, soil-moisture sensors, extensometers and displacement instruments for particularly hazardous slopes. These operational systems demonstrate that rainfall thresholds can provide effective warnings where dense observational infrastructure exists; however, their dependence on extensive radar or gauge networks restricts applicability in mountainous regions where monitoring infrastructure is sparse or absent. Besides national- and regional-scale operational networks, numerous local-scale, site-specific landslide early warning systems rely on dense rain gauge networks and locally calibrated susceptibility models. For instance, the Slope Instability Predictor–Kerala (SLIP-K) is a web-based and mobile-enabled early warning system developed for parts of the Kerala region of the Western

https://doi.org/10.5194/egusphere-2026-4588
Preprint. Discussion started: 21 August 2026

Ghats, where landslide forecasts are generated using gauge-based rainfall observations and local susceptibility information (Mohan et al., 2026). However, the deployment of dense real-time rain gauge networks remains highly uneven, with many countries in the Global South and other developing regions characterized by sparse monitoring infrastructure, discontinuous observations, and limited maintenance, thereby constraining the implementation of operational landslide early warning systems.

To overcome the limitations of ground-based observations, satellite precipitation products have increasingly been incorporated into landslide hazard assessment. One of the earliest quasi-global demonstrations was presented by Hong et al. (2006), who showed that precipitation estimates from NASA's Tropical Rainfall Measuring Mission (TMPA) could reproduce spatial and temporal patterns associated with landslide occurrence. Nevertheless, this framework still required regional calibration and therefore lacked global transferability. Other global-scale studies have mapped landslide susceptibility (Nadim et al., 2006; Dixit et al., 2024; Yunus et al., 2021) or retrospectively reconstructed rainfall-triggered hazard patterns (Farahmand & AghaKouchak, 2013), but these products were not designed for continuous operational forecasting.

A major advance came with the development of the Landslide Hazard Assessment for Situational Awareness (LHASA) (Stanley & Kirschbaum, 2017; Kirschbaum & Stanley, 2018). LHASA represented the first globally available near-real-time satellite-based landslide nowcasting framework by combining low-latency IMERG precipitation with a global susceptibility model to identify locations where rainfall-triggered landslides were more likely to occur (Kirschbaum et al., 2015; Stanley & Kirschbaum, 2017). The system significantly improved global situational awareness by exploiting publicly available satellite observations and operating without reliance on national gauge networks. Subsequent versions (LHASA Version 2) replaced the static susceptibility map with a machine-learning framework incorporating multiple environmental predictors, together with dynamic variables such as soil moisture and snow cover, thereby improving global prediction skill (Stanley et al., 2021).

Despite these advances, important limitations remain. First, LHASA is fundamentally a nowcasting system rather than a forecasting system because it relies on IMERG Early and Late precipitation products with typical latencies of approximately 4–18 hours. Consequently, alerts, when issued, are based on rainfall that has already occurred, substantially reducing the lead time available for emergency preparedness and evacuation. Second, although LHASA Version 2 incorporates additional environmental predictors, it primarily estimates landslide hazard and does not explicitly quantify exposure or potential impact on populations and infrastructure. Third, the framework provides generalized global assessments that cannot readily accommodate locally calibrated rainfall thresholds or regional susceptibility models capable of improving hazard assessment in individual mountain regions. An experimental effort by Khan et al. (2021) incorporated rainfall forecasts into LHASA using

https://doi.org/10.5194/egusphere-2026-4588
Preprint. Discussion started: 21 August 2026

GOES forecast products, illustrating the feasibility of predictive landslide forecasting; however, this approach has not developed into a widely operationalized forecasting system.

These limitations highlight a critical gap in the evolution of operational landslide early warning systems. Existing national systems provide reliable forecasts but require dense observational infrastructure that is unavailable across much of the Global South, whereas global satellite systems provide near-real-time situational awareness but offer limited forecasting capability and limited consideration of exposure and risk. As a result, there remains a need for globally transferable operational framework that simultaneously integrates satellite observations, numerical weather prediction, locally calibrated rainfall thresholds, susceptibility modelling, and exposure information into an actionable forecasting system.

The proposed Automated Landslide Early Risk Tracker (ALERT) framework is designed to address this gap. ALERT extends beyond existing satellite nowcasting approaches by integrating near-real-time IMERG observations with bias-corrected numerical weather prediction rainfall forecasts, enabling forecast-based rather than observation-based hazard assessment. The framework dynamically evaluates rainfall threshold exceedance using regionally calibrated intensity–duration thresholds while combining these forecasts with high-resolution susceptibility models, terrain information, runout assessment, and exposure datasets to estimate potential impacts on settlements and infrastructure. Implemented within a cloud-native architecture, ALERT provides a scalable and transferable early warning capability for data-sparse mountainous regions where conventional gauge-based systems are impractical.

3 ALERT Architecture

ALERT is designed as a modular, cloud-native landslide early warning architecture capable of operating across diverse climatic and geomorphic environments using globally available rainfall hindcast and forecast products and regionally calibrated rainfall thresholds. The framework combines four principal components: (i) rainfall hindcast and forecast data; (ii) intensity–duration threshold exceedance analysis; (iii) susceptibility-constrained hazard classification; and (iv) runout and exposure assessment. All computational workflows are implemented within the Google Earth Engine (GEE) cloud environment, enabling near-real-time hazard analytics without dependence on local computational infrastructure. ALERT integrates these components into a unified mapping between environmental forcing and decision-support products. The detailed workflow of ALERT framework is shown in Figure 1.

https://doi.org/10.5194/egusphere-2026-4588
Preprint. Discussion started: 21 August 2026

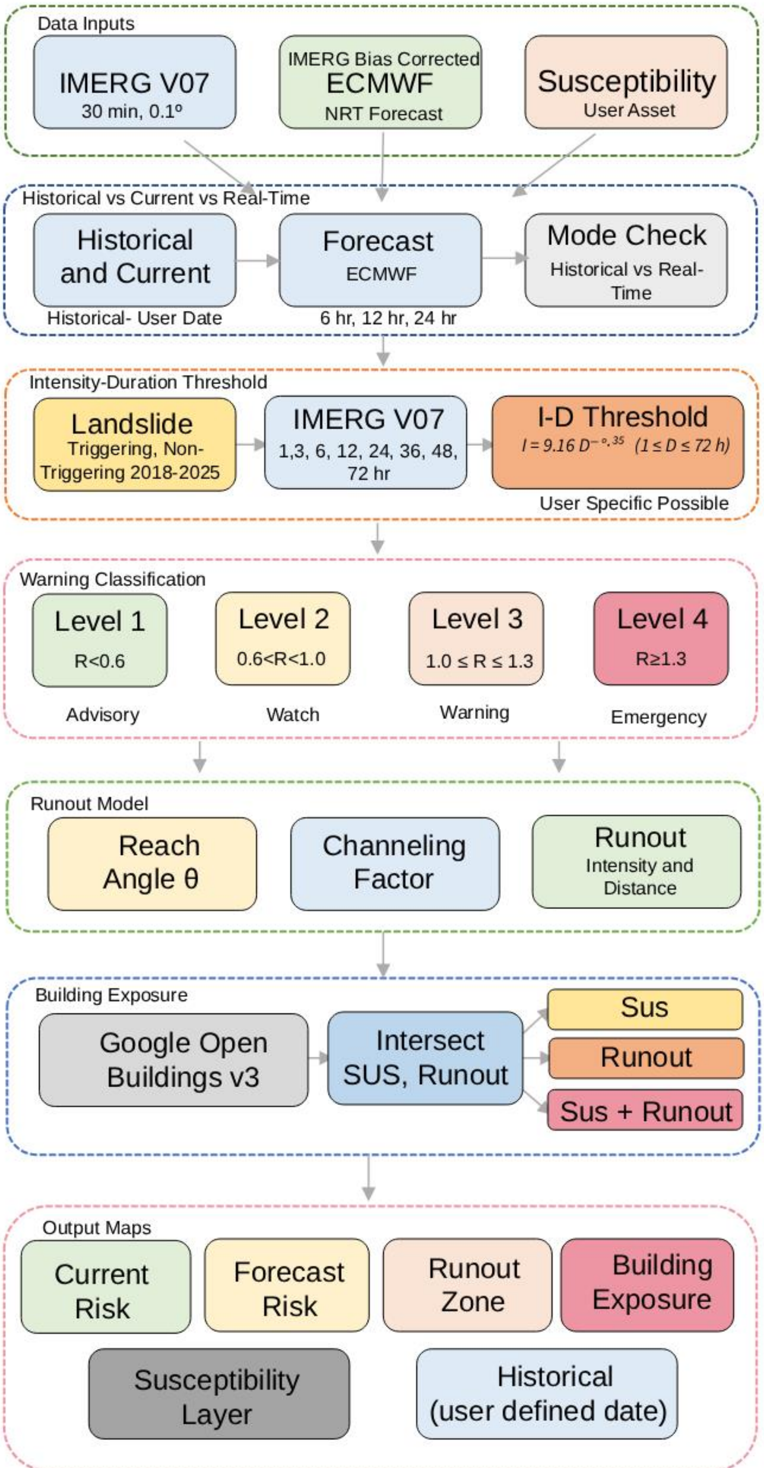

https://doi.org/10.5194/egusphere-2026-4588
Preprint. Discussion started: 21 August 2026

Figure 1. Flowchart illustrating the detailed methodology of the ALERT landslide early warning framework.

3.1 Satellite rainfall for hindcast and forecasts

NASA's IMERG Final Run product (Version 07, NASA/GPM_L3/IMERG_V07) and the ECMWF Integrated Forecasting System (IFS) Operational near real-time (NRT) product hosted on GEE (ECMWF/NRT_FORECAST/IFS/OPER) are the primary rainfall datasets used in ALERT, providing precipitation estimates at 0.1° and 0.25° spatial resolutions, respectively. The IMERG dataset integrates passive microwave retrievals, infrared-based rainfall rates, and monthly rain gauge analyses from the Global Precipitation Climatology Centre (GPCC) to produce a quasi-global, gauge-adjusted estimate (Huffman et al., 2019). The precipitation band retrieved from each 30-minute IMERG granule carries units of mm hr^{-1}. To convert these rates to hourly rainfall, each image is multiplied by a factor of 0.5 h.

ALERT operates in two distinct modes depending on user input. When a specific historical date is provided, the system enters hindcast mode, anchoring the analysis end time to midnight of the following day and stepping back exactly 24 hours to define the observation window. When no date is supplied, the system enters real-time mode, anchoring the end time to the current UTC time. In both cases, the analysis window is a rolling 24-hour period ending at the reference time. This dual-mode architecture allows the system to be used either for post-event validation and mapping or for operational near-real-time monitoring.

For hindcast analysis, precipitation is sourced from the IMERG. Accumulation totals for 24, 12 and 6 h are computed from the IMERG hourly rainfall to capture both short-duration convective events and prolonged synoptic rainfall. In real-time mode, precipitation forecasts are obtained from the ECMWF Integrated Forecasting System (IFS) Operational near real-time (NRT) archive hosted on GEE (ECMWF/NRT_FORECAST/IFS/OPER), providing total precipitation fields at approximately 0.25° resolution. The ECMWF IFS medium-range control forecast is initialized four times daily (00, 06, 12, and 18 UTC). The forecast precipitation field is sourced from the *total_precipitation_sfc* band, which provides accumulated precipitation at the surface in meters. A correction factor of 1000 is applied to convert meters to millimeters. ALERT identifies the most recently available forecast cycle within a predefined temporal search window and uses the system:time_start attribute as the initialization time of that cycle. All forecast steps belonging to the selected cycle are subsequently isolated using this initialization time.

Because ECMWF total precipitation is provided as a cumulative quantity from the beginning of each forecast cycle, the rainfall expected over a future forecast horizon cannot be obtained directly from a single forecast step once the forecast cycle has already progressed. ALERT therefore accounts for the elapsed time between forecast initialization and the current model-evaluation time. A baseline forecast step is selected as the first available forecast step at or after the current elapsed forecast time, thereby providing a cumulative precipitation value representative of the current state of the forecast cycle. For a forecast horizon of (H) hours, the target is defined as the earliest available forecast step at or beyond the elapsed time plus (H). Forecast

https://doi.org/10.5194/egusphere-2026-4588
Preprint. Discussion started: 21 August 2026

rainfall accumulated over the next (H) hours is then calculated from the difference between the cumulative precipitation at the target and baseline steps.

Raw ECMWF forecasts exhibit systematic biases relative to IMERG climatology, particularly in orographically complex terrain (Beljaars et al. 2005). To ensure dynamical consistency between the threshold calibration domain (IMERG) and the forecast domain (ECMWF), we compute a spatially explicit bias correction factor using the ratio of long-term mean monthly IMERG totals to corresponding ECMWF precipitation climatology, generating a pixel-wise multiplicative correction layer applied to all forecast fields within ALERT. This correction accounts for systematic regional biases between ECMWF model climatology and IMERG rainfall estimates. Currently, for the global landslide susceptibility layer, pixels are unmasked using a multiplicative factor of 1.0, preserving the raw ECMWF values. Nevertheless, the model allows the users to provide a bias asset for their defined study geometry.

To operationalize the threshold within ALERT, a dimensionless exceedance ratio R is computed for each pixel:

$$R(D) = \frac{I_{obs}(D)}{aD^{-b}}$$

where $I_{obs}(D)$ is the mean observed or forecast rainfall intensity over duration D at the pixel centre. $R \geq 1$ indicates threshold exceedance. The maximum of R(6), R(12) and R(24) is taken as the composite triggering index for the current observation or forecast period, reducing sensitivity to the choice of a single reference duration. The exceedance ratio is then discretized into four ordinal rainfall hazard classes (see Section 5). The resulting rainfall hazard class is then coupled with the pixel-wise terrain susceptibility class (1–5).

3.2 Intensity Duration thresholds

A central feature of ALERT is the integration of a globally interoperable threshold catalogue that dynamically deploys region-specific rainfall threshold parameters across multiple mountain systems. Rather than relying on a single globally fixed threshold, the framework dynamically deploys regional rainfall threshold parameters according to climatic and geomorphic context. The operational pipeline therefore remains identical across regions, while only the threshold coefficients and susceptibility layers vary geographically. This design allows ALERT to function as a globally transferable hazard forecasting system while preserving regional hydroclimatic sensitivity. The framework currently incorporates published thresholds representing tropical monsoon environments, humid subtropical regions, alpine terrains, and continental mountain systems, including thresholds from India, Japan, Italy, China, South Korea, Malaysia, Sri Lanka, the European Alps, and other globally derived compilations (Table 1). The ID threshold rainfall exceedance works in the following fashion:

Table 1. Intensity-Duration (ID) threshold currently available in the ALERT framework. Note that any new ID values can be incorporated by typing manually the a and b coefficients.

S No.	Region	Source	a	b
1	India – Western Ghats (default)	This Study	9.16	−0.35
2	Global	Caine (1980)	14.82	−0.39
3	Global	Guzzetti et al. (2007)	2.20	−0.44
4	Global	Jia et al. (2020)	2.57	−0.48
5	Italy	Guzzetti et al. (2025)	5.30	−0.61
6	Italy	Brunetti et al. (2010)	12.17	−0.64
7	Italy	Peruccacci et al. (2017)	7.70	−0.61
8	CADSES Europe	Guzzetti et al. (2007)	9.40	−0.56
10	Japan	Jibson (1989)	39.71	−0.62
11	Japan	Saito et al. (2010)	2.18	−0.26
12	India – Darjeeling/Sikkim	Mandal & Sarkar (2020)	20.10	−0.45
13	India – Sikkim	Harilal et al. (2019)	43.26	−0.78
14	India – Wayanad	Abraham et al. (2020)	2.09	−0.24
15	India – Idukki	Abraham et al. (2019)	0.90	−0.16
16	India – Kashmir	Shah et al. (2024)	1.1953	−0.352
17	South Korea	Kim et al. (2020)	10.40	−0.31
18	China – Zhejiang	Ma et al. (2015)	52.86	−0.45
19	China	He et al. (2020)	0.53	−0.30
20	Slovenia	Jordanova et al. (2020)	6.80	−0.60
21	Malaysia	Maturidi et al. (2021)	17.50	−0.722
22	Sri Lanka	Nawagamuwa & Perera (2017)	14.02	−0.30
23	France – Alps	Barthélemy et al. (2025)	8.29	−0.69
24	Spain – Pyrenees	Oorthuis et al. (2023)	11.03	−0.75

https://doi.org/10.5194/egusphere-2026-4588
Preprint. Discussion started: 21 August 2026

For a rainfall duration D (hours), the empirical ID threshold intensity is:

$$I_{\{crit\}}(D) = aD^{b}, b < 0$$

with region-specific coefficients (a,b) drawn from the literature preset table (e.g. Western Ghats: a= 9.16 and b = -0.35). Observed rainfall accumulation (P in mm) is obtained by summing IMERG rainfall rates over the trailing window of length D:

$$P_D(x,y) = \sum_{t=t_0-D}^{t_0} \mathrm{r(x,y,t)}\ \Delta t, \quad \Delta t = 0.5$$

the mean intensity over that window is:

$$I_D = \frac{P_D}{D}$$

and the exceedance ratio is:

$$R_D(x,y) = \frac{\bar{I}_D(x,y)}{I_{crit}(D)} = \frac{P_D(x,y)}{D\,.\,a.\,D^b}$$

Durations (D=6, 12 and 24 h) are also evaluated in parallel to capture short intense bursts and longer sustained rainfall; the governing (most critical) ratio is:

$$R = \max(R_6, R_{12}, R_{24})$$

Thus, R=1 represents rainfall conditions equal to the empirical landslide-triggering threshold, R<1 represents rainfall below the threshold, and R>1 represents threshold exceedance. For the forecast branch, the same ratio is computed from ECMWF cumulative precipitation difference between forecast steps,

$$P_D^{fc}(x,y) = \left[\,\hat{P}(t_0 + D) - \hat{P}(t_0)\right]_+ \cdot 1000 \cdot \beta(x,y)$$

where $\hat{P}$ is the cumulative total precipitation (m) from a single forecast run, the factor 1000 converts m→mm, and $\beta(x,y)$ is the bias-correction field and same is disabled now in GLS mode.

3.3 Susceptibility Framework in ALERT

https://doi.org/10.5194/egusphere-2026-4588
Preprint. Discussion started: 21 August 2026

ALERT incorporates both regional and global susceptibility frameworks. For the Western Ghats validation domain, a deep neural network (DNN)-derived susceptibility model previously developed using 16 geo-environmental variables was implemented (Achu et al., 2024). These variables included topographic, hydrological, geological, and rainfall-related predictors derived from SRTM topography and ancillary datasets. Variable selection was performed using multicollinearity analysis, and model optimization employed training–testing splits and cross-validation procedures. The resulting susceptibility probabilities were classified into five ordinal classes: very low, low, moderate, high, and very high susceptibility. The regional DNN framework achieved receiver operating characteristic (ROC) area-under-curve (AUC) values exceeding 0.9, indicating strong predictive skill.

For global deployment, ALERT incorporates NASA-derived 1-km global landslide susceptibility layer (Figure 2) (Stanley, and Kirschbaum, 2017). The framework permits users to dynamically switch between regional high-resolution susceptibility assets and globally available susceptibility baselines, as well as user-specified assets thereby enabling transferability across ungauged mountain systems**.**

Similar to the regional LEWS proposed by Piciullo et al. (2017), ALERT employs multiple calibrated warning levels instead of a single rainfall threshold. To generate operational warning levels by integrating rainfall forcing and terrain susceptibility, ALERT first converts the rainfall threshold exceedance ratio (R) into an ordinal rainfall class (C_R):

$$C_R = \begin{pmatrix} 1 & if & R < 0.6 \\ 2 & if & R \leq 0.6 < 01 \\ 3 & if & R \leq 1 < 1.3 \\ 4 & if & R \geq 1.3 \end{pmatrix}$$

These rainfall classes are referenced to the physically meaningful threshold of R=1, which represents rainfall equal to the empirical intensity–duration (I–D) threshold for landslide initiation. A precautionary *Watch* level ($0.6 \leq R < 1.0$) is introduced to provide early situational awareness as rainfall approaches the critical threshold, while an *Emergency* level ($R \geq 1.3$) represents rainfall exceeding the threshold by at least 30%, indicating increased triggering potential. Such multi-level warning classification is well established in operational LEWS. Nevertheless, ALERT defines warning classes using the rainfall threshold exceedance ratio and further constrains the final warning level using terrain susceptibility, thereby integrating both dynamic triggering conditions and static predisposing factors. This ensures that areas of low susceptibility ground cannot reach the highest alert classes even under extreme rainfall.

$$W = \min\left(C_R, f(s)\right), \quad f(S) = \begin{pmatrix} 2 & if & S \leq 2 \\ 3 & if & S = 3 \\ 4 & if & S \geq 4 \end{pmatrix}$$

https://doi.org/10.5194/egusphere-2026-4588
Preprint. Discussion started: 21 August 2026

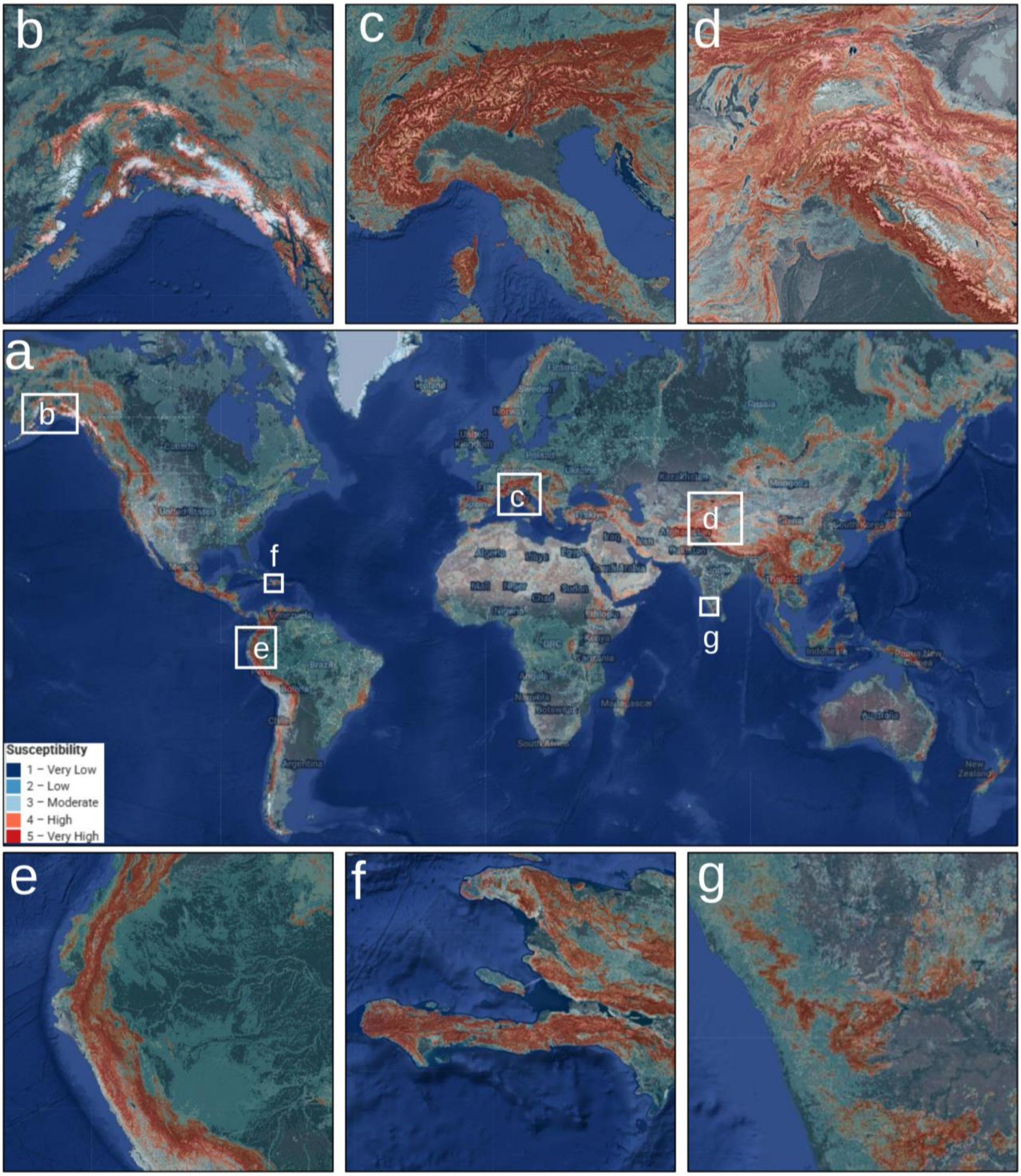

Figure 2. (a) Global landslide susceptibility map sourced from Stanley and Kirschbaum, (2017). Inset showing the zoomed areas in parts of (b) Alaska, (c) Italy, (d) North-Western Himalaya, (e) Andes, (f) Haiti and (g) Western Ghats.

https://doi.org/10.5194/egusphere-2026-4588
Preprint. Discussion started: 21 August 2026

3.4 Runout Model and Building Exposure Addons

Along with landslide susceptibility-based warnings, a flow runout model is also implemented as an add-on module. The runout is estimated using the empirical reach angle (Fahrböschung) method, which relates the elevation drop and horizontal distance to define the potential flow extent. For each pixel exceeding a predefined warning threshold, the travel angle between an upslope source and a downslope receiver was calculated as the ratio of the height difference (ΔH) to the planimetric distance (D). Given a binary source mask pixels M(x,y) = 1 for pixels where [$W(x,y) \geq L_{trig}$] (i.e., pixel at or above the trigger level), the model searches, within a radius r_{max}, for the elevation drop and planimetric distance to the nearest source pixel:

The apparent reach (Fahrböschung) angle is:

$$\boldsymbol{\theta} = \mathbf{arctan}\left(\frac{\mathbf{\Delta H}}{\mathbf{D}}\right) \times \left(\frac{\mathbf{180}}{\boldsymbol{\pi}}\right)$$

where ΔH is the height drop from the highest upslope source pixel within the search radius to the receiver pixel, and D is the horizontal planimetric distance between them. A default reach angle of $\boldsymbol{\theta eff}$ =11° is adopted, representing typical channelised debris flow behaviour in the Western Ghats (Islam et al., 2025), while allowing flexibility for different flow types.

A pixel enters the runout zone if the following conditions hold:

$$\boldsymbol{Runout}(\boldsymbol{x},\boldsymbol{y}) = \mathbf{1}[\boldsymbol{\theta} \geq \boldsymbol{\theta eff}] \cdot \mathbf{1}[\boldsymbol{\Delta H} > \mathbf{0}]$$

Provisions for adjusting the threshold are provided in the GEE interface. To account for enhanced mobility of debris flows within confined drainage networks, a flow-channeling correction was also incorporated (cf. Rickenmann, 2005). This modification reduces the effective reach angle as a function of upstream flow accumulation, reflecting reduced frictional resistance and lateral spreading in channelized conditions.

Building data are assessed using Google Open Buildings v3, a global dataset of machine-learning detected building footprints (Sirko et al., 2021). Building exposure categories are then derived by pixel-wise intersection of the building presence raster

https://doi.org/10.5194/egusphere-2026-4588
Preprint. Discussion started: 21 August 2026

with the runout zone and susceptibility raster. Given the runout binary mask Z, susceptibility class S, and building confidence raster $B_c(x,y)$, the corresponding exposure classes are derived as follows:

$$\boldsymbol{B}(\boldsymbol{x},\boldsymbol{y}) = \mathbf{1}[\boldsymbol{B}_{\boldsymbol{c}}(\boldsymbol{x},\boldsymbol{y}) > \mathbf{0}]$$

The detailed flowchart of the methods and GEE architecture is presented in Figure 1.

4 ALERT framework Testbed

To calibrate and validate the framework, the Western Ghats of India were selected as a benchmark domain because of their strong monsoonal rainfall gradients, recurrent debris-flow activity, and availability of a multi-year landslide inventory. The Western Ghats of India, a UNESCO World Heritage biodiversity hotspot extending approximately 1,600 km along the western coast of the Indian subcontinent, provide an ideal testbed, exemplifying the convergence of natural susceptibility and societal vulnerability that motivates the development of satellite-driven landslide early warning systems (Yunus et al., 2021). The region experiences some of the highest rainfall intensities in the world during the southwest monsoon (June–September), regularly exceeding 3,000 mm per season in windward escarpment zones, and is subject to recurrent catastrophic landslide events that disproportionately affect rural and indigenous communities (Achu et al. 2025).

The Western Ghats (8°–21°N, 73°–77°E) form an elongated mountainous escarpment, covering approximately 160,000 km² across the states of Maharashtra, Goa, Karnataka, Kerala, and Tamil Nadu (Figure 3). Elevations range from sea level to over 2,695 m at Anamudi in the southern part of the Ghats. The terrain is characterized by steep gradients, deeply incised river valleys, lateritic and crystalline basement geology, and dense tropical evergreen forest that grades into deciduous woodland at higher elevations (Achu et al. 2024, 2025; Yunus et al. 2025).

The region experiences a pronounced seasonal climate dominated by the southwest monsoon (June–September), during which orographic enhancement produces extreme rainfall in parts of Kerala, coastal Karnataka, and the Western Ghats of Maharashtra. Post-monsoon cyclonic systems further contribute to high-intensity rainfall events in the southern sector. This rainfall regime, superimposed on steep, weathered slopes, creates favorable preconditions for rainfall-triggered shallow translational landslides, debris flows, and rock falls (Achu et al. 2025). Recent years have witnessed a marked increase in reported landslide frequency, likely attributable to a combination of extreme precipitation events, land-use change, and improved event reporting (Islam et al., 2025).

4.1 Landslide Inventory and Susceptibility Map for Western Ghats

We compiled a regional landslide inventory for the Western Ghats spanning the period January 2018 to December 2025, comprising over 5474 landslides. Landslide polygon boundaries were mapped manually from high-resolution archived satellite

https://doi.org/10.5194/egusphere-2026-4588
Preprint. Discussion started: 21 August 2026

imagery available through Google Earth. While most of these landslides are triggered during extreme events of 2018, 2019, and 2021 in the Western Ghats, some isolated events, including those in 2024, are also incorporated. Additionally, we accessed the Bhusanket portal (https://www.bhusanket.gsi.gov.in/) of the Geological Survey of India (GSI) and added 7707 point-based landslides, bringing the total to 13188 landslides (Figure 3).

Among these, 104 landslides have verified dates of occurrence, enabling direct linkage with satellite-derived rainfall time series. For the majority of events where precise timing is unavailable, landslide initiation was approximated by assigning the hour of peak rainfall on the corresponding event day. While this assumption introduces uncertainty, it provides a consistent and pragmatic approach for temporal alignment with rainfall forcing, facilitating subsequent analysis of I-D relationships at the WG scale.

For the development of the landslide susceptibility map (LSM) asset within the ALERT application, a subset of the GSI dataset, originally implemented using a deep neural network (DNN) framework in R® programming environment, was utilized in this study. The modelling framework for LSM generation employed a multi-layer neural network with optimized hyperparameters (cf. Achu et al. 2024), using a combination of training–testing splits and cross-validation to ensure reliability. Sixteen geo-environmental variables, including elevation, rainfall, lithology, and other terrain indices derived from the SRTM DEM, were prepared for the LSM generation using the DNN framework. Multicollinearity analysis was performed on the variables using statistical measures such as variance inflation factor (VIF), tolerance, and correlation coefficients in which the highly correlated variable, such as topographic ruggedness, was excluded from further analysis due to its high correlation with slope. Variable importance shows slope topographic wetness and distance to stream have the highest control on landslide occurrence. The

https://doi.org/10.5194/egusphere-2026-4588
Preprint. Discussion started: 21 August 2026

ROC under AUC values for the modeled was found to be over 0.9. The output probability maps were classified into five levels namely very low, low, moderate, high, and extreme classes based on the equal interval method (Figure 4).

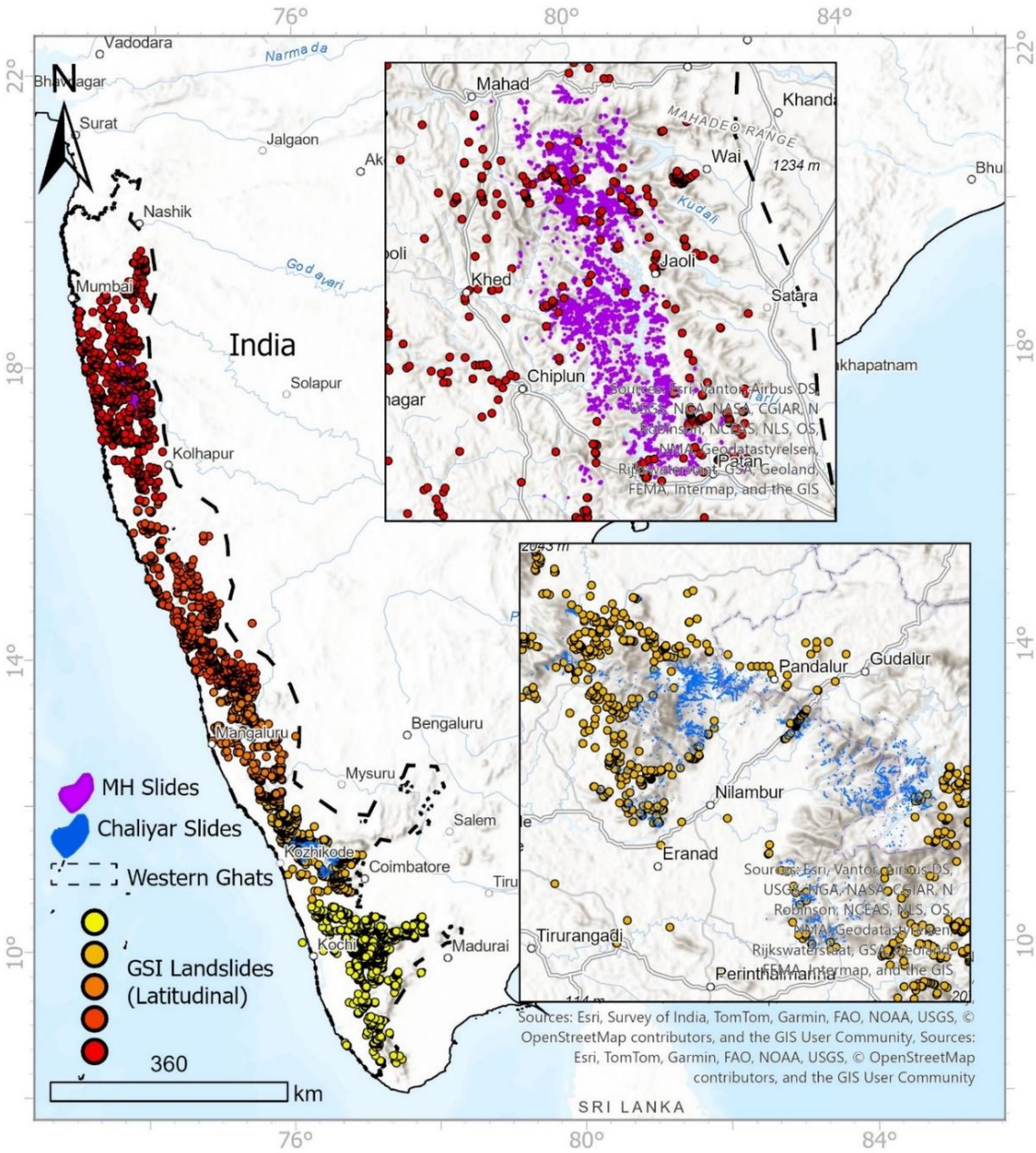

Figure 3. Study area map of southern India showing the extent of the Western Ghats, with landslides mapped by GSI (points) and additional inventories developed in this study (blue and purple polygons) (Sources: Esri, Survey of India, TomTom, Garmin, FAO, NOAA, USGS, OpenStreetMap | Powered by Esri).

https://doi.org/10.5194/egusphere-2026-4588
Preprint. Discussion started: 21 August 2026

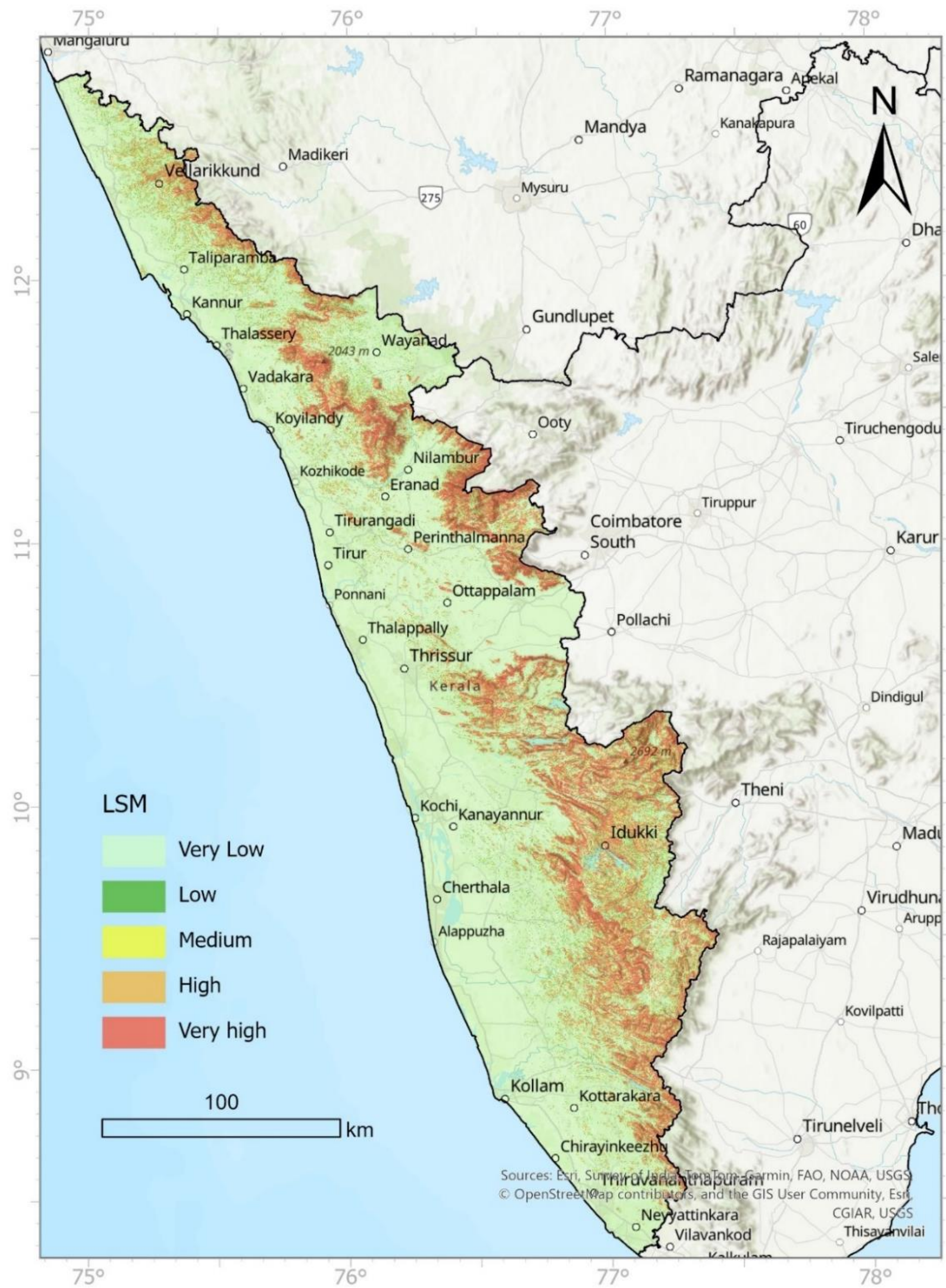

Figure 4. Landslide susceptibility map of the southern Western Ghats generated using a deep learning framework with 16 geo-environmental variables at 100 m spatial resolution (Sources: Esri, Survey of India, TomTom, Garmin, FAO, NOAA, USGS, OpenStreetMap | Powered by Esri).

https://doi.org/10.5194/egusphere-2026-4588
Preprint. Discussion started: 21 August 2026

4.2 Rainfall I-D Threshold

For each landslide event, defined by its recorded longitude, latitude, date and time, we extracted precipitation time series from the IMERG's 0.1° grid cell encompassing the reported location for the 72 hours preceding the event, enabling the derivation of antecedent and triggering rainfall variables across durations of 1 to 72 hours. For landslide events without time information, we selected the peak value of 24-h rainfall during the event day as the approximate initiation time, consistent with previous studies. To construct a paired dataset of triggering and non-triggering rainfall episodes, necessary for threshold discrimination and skill assessment, two additional temporal windows were extracted for each landslide site by shifting the failure date by ±15 days. These off-event windows sampled the same location under similar seasonal climatological conditions but in the absence of a recorded failure, providing the non-triggering counterparts drawn from the same monsoon period. Additional random dates during the monsoon periods of previous years were added to the non-triggering events.

For each landslide event and paired non-triggering rainfall episode, antecedent rainfall intensities were extracted at seven standard accumulation windows: 1, 3, 6, 12, 24, 48, and 72 hours yielding a multi-duration intensity matrix indexed by site and event label (triggering: label = 1; non-triggering: label = 0). To establish rainfall thresholds, a log–log transformation of intensity and duration was performed, and an ordinary least squares (OLS) regression was applied to the triggering rainfall dataset. This yielded a power-law relationship of the form $I=a.D^b$, representing the I–D threshold for the WG. Uncertainty in the fitted relationship was quantified using a 95% confidence interval derived from residual statistics. Additionally, a mean-envelope threshold was defined, providing an additional upper-envelop threshold for landslide initiation. The derived thresholds were further compared with established global thresholds (Caine, 1980; Guzzetti et al., 2007, 2025) to assess their applicability to tropical settings.

Empirical rainfall ID thresholds were derived using a frequentist approach adapted to satellite rainfall. For each landslide event in the inventory (n = 104), the mean rainfall intensity over durations D = 1, 3, 6, 12, 24, 48, and 72 hours prior to the reported landslide time was extracted from the co-located IMERG pixel. The resulting (D, I) pairs were plotted in log-log space, where power-law behaviour produces a linear relationship:

$$log(I) = log(\alpha) + \beta \cdot log(D)$$

Threshold estimation was performed using least-squares regression on the lower 10th percentile of the empirical (I-D) distribution for each duration class, yielding a conservative lower-bound threshold that reduces the likelihood of false negatives (Figure 5). The derived conservative threshold for the Western Ghats is:

$$I = 9.16\, D^{-0.35}\ (I \leq D \leq 72h)$$

https://doi.org/10.5194/egusphere-2026-4588
Preprint. Discussion started: 21 August 2026

where (I) is in mm h⁻¹, and (D) is expressed in hours. This relationship indicates that rainfall intensities associated with landslide triggering decrease with increasing duration, consistent with the role of antecedent soil moisture in prolonged events. The parameters $\alpha = 9.16$ and $\beta = -0.35$ fall within the range reported for humid tropical regions (Guzzetti et al., 2025; Kim et al., 2020; Mandal & Sarkar, 2020), lending confidence to the satellite-derived calibration.

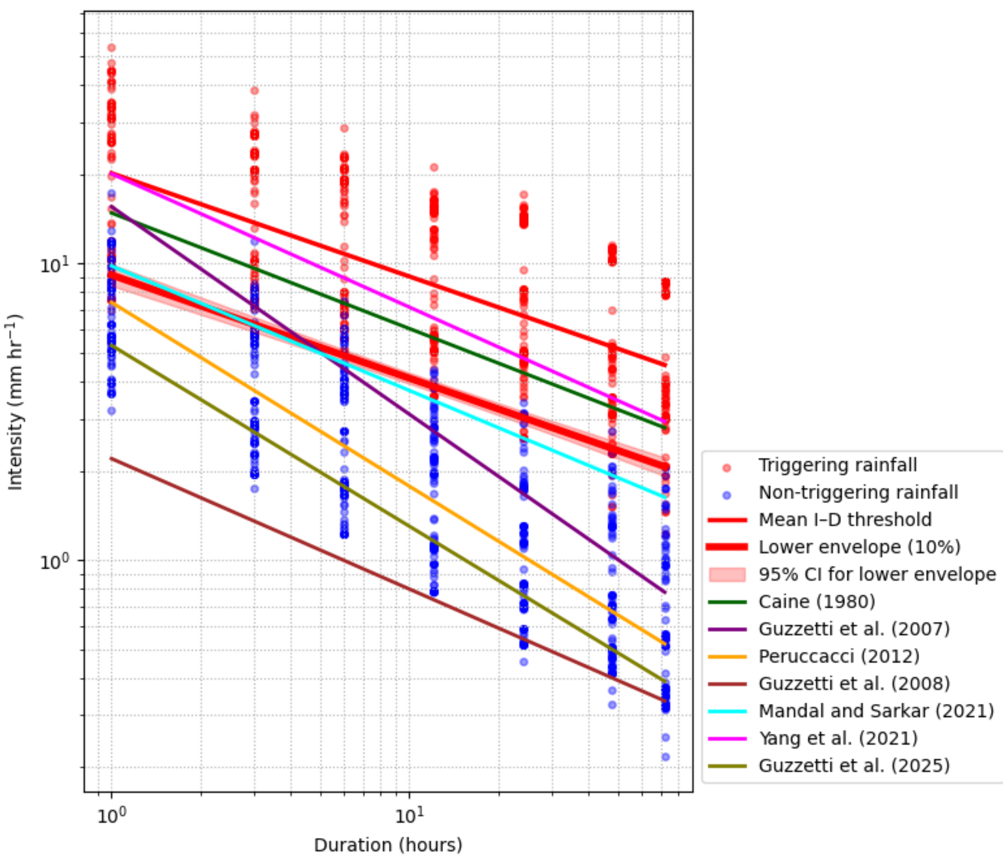

Figure 5. Rainfall intensity–duration (I–D) relationship for landslide-triggering and non-triggering events plotted in log–log space. The derived regional I–D threshold (solid red line) and corresponding 95% confidence interval (shaded band) are shown along with the mean-threshold (red upper line). Global thresholds proposed by Caine (1980), Guzzetti et al. (2007), and other studies are included for comparison.

4.3 Validation

The performance of ALERT was evaluated independently of the threshold calibration using dated landslide events from the Western Ghats inventory. A total of 104 landslides with verified event dates were available for direct temporal comparison

https://doi.org/10.5194/egusphere-2026-4588
Preprint. Discussion started: 21 August 2026

with satellite-derived rainfall. To minimize spatial sampling bias, each landslide location was retained as the spatial sampling unit, while non-landslide samples were generated at the same locations using randomly selected dates within the monsoon period on which no landslide was recorded. Dates occurring within ±3 days of any documented landslide event were excluded from the control pool to reduce the possibility of contamination by rainfall associated with the event. This paired design therefore emphasizes temporal discrimination between landslide and non-landslide rainfall conditions rather than differences in terrain susceptibility.

ALERT predictions were converted into binary event/non-event classifications for validation, with an alert condition defined as W≥3 (Warning or Emergency) and a non-alert condition defined as W<3 (Advisory or Watch). Model performance was evaluated using the confusion matrix and the following metrics: probability of detection (POD), false-alarm ratio (FAR), precision, specificity, F1 score, critical success index (CSI), accuracy, and true skill statistic (TSS).

5 Results

5.1 ALERT Warnings

ALERT produces a four-level hazard classification scheme, in which rainfall conditions remain below the empirical triggering threshold when (R<1), whereas threshold exceedance, and hence an increased potential for landslide occurrence, is indicated when (R≥1). Advisory corresponds to R<0.6, indicating rainfall substantially below the empirical triggering threshold. Watch corresponds to 0.6≤R<1.0, representing conditions approaching the threshold and providing precautionary situational awareness. Warning corresponds to 1.0≤R<1.3, indicating that the empirical rainfall threshold has been exceeded. Emergency corresponds to R≥1.3, representing rainfall exceeding the threshold by at least 30%. These classes are intended as operational decision categories rather than probabilistic estimates of landslide occurrence (Table 2). The progressive warning levels reflect the increasing severity of rainfall conditions relative to the empirical threshold and, consequently, an expected increase in the likelihood of rainfall-induced failure (Caine, 1980; Guzzetti et al., 2007).

Table 2. Warning schema implemented in the ALERT framework

Level	Name	R Threshold
1 – Green	Advisory	R < 0.6
2 – Yellow	Watch	0.6 ≤ R < 1.0
3 – Orange	Warning	1.0 ≤ R < 1.3
4 – Red	Emergency	R ≥ 1.3

The rainfall-derived warning class R_{class} is subsequently constrained by the susceptibility class S_{class} to obtain the final warning level (W). Susceptibility classes range from 1 (very low) to 5 (very high), while the rainfall warning output contains

https://doi.org/10.5194/egusphere-2026-4588
Preprint. Discussion started: 21 August 2026

four levels. To maintain operational consistency and avoid issuing disproportionately high warnings in areas of low susceptibility, susceptibility classes 1–2 permit a maximum output of Watch (level 2), class 3 permits a maximum output of Warning (level 3), and classes 4–5 permit the full four-level warning range. The final warning level is therefore determined conservatively as

$$W = \min\,(R_{class}, S_{class})$$

where R_{class} is the rainfall-derived class, and S_{class} is the corresponding susceptibility-based maximum warning class.

$$S_{class} = \begin{cases} 2, & S = 1, 2 \\ 3, & S = \quad 3 \\ 4, & S = 4, 5 \end{cases}$$

This conditional logic provides a simple mechanism for integrating rainfall forcing with spatial susceptibility while limiting the escalation of warnings in areas where the underlying susceptibility to landsliding is low. In the validation section presented here, this susceptibility-constrained approach substantially reduced false-alarm rates in areas characterized by gentle relief. Previously, Segoni et al. (2015) proposed such a multi-tier decision scheme in which increasing rainfall criticality progressively extended the warning to areas of lower susceptibility, based on the premise that increasingly severe rainfall can overcome progressively lower levels of terrain predisposition.

5.2 Google Earth Engine Application Architecture and Interface

ALERT is implemented as a GEE JavaScript API application (Code Editor script) accessible via a public URL https://ee-yunuscool.projects.earthengine.app/view/alert-app. The architecture consists of two main parts: (i) a data ingestion module, which retrieves IMERG images for user-selected dates (or defaults to current UTC time) and aggregates 6-hour and 24-hour rainfall sums using image collection filtering and map-reduce operations. (ii) a hazard computation module, which applies the ID threshold equation pixel-wise to produce the exceedance ratio R, classifies R into the four-level warning scheme, and constrains the output by the susceptibility layer. In forecast mode, ECMWF NRT images for 6-, 12-, and 24-hour lead times are retrieved, with bias correction applied to the Western Ghats region on the fly by multiplying the forecasts by the pre-computed correction raster asset. The output is displayed as a colour-coded map with four warning levels: Advisory (green), Watch (yellow), Warning (orange), and Emergency (red) (Table 1).

Figure 6 shows an example using the global susceptibility layer and the Western Ghats-derived threshold. Large portions of the Indian Peninsula, including the Western Ghats region, are classified as Advisory level, indicating that rainfall conditions on 22 July 2026 at 06:46:43 GMT were below the critical threshold for landslide initiation. This indicates relatively stable slope conditions at the time of analysis, with no widespread triggering expected. By default, the system uses the WG threshold

https://doi.org/10.5194/egusphere-2026-4588
Preprint. Discussion started: 21 August 2026

($I = 9.16 \cdot D^{-0.35}$) to evaluate rainfall conditions in near-real-time. Based on this threshold, the model dynamically updates warning levels depending on rainfall exceedance. Nevertheless, parts of the northwestern Himalayas, 24-hour rainfall exceeded 100 mm, were classified in some grid cells as Warning or Emergency, indicating hazardous rainfall conditions during the analysis period. All computations are performed on GEE's cloud infrastructure, ensuring that only the spatial extent visible in the user's map viewport is computed at any given time. All the computations are performed on GEE's cloud infrastructure, ensuring that only the spatial extent visible in the user's map viewport is computed at any given time. A notable feature of the ALERT framework is its flexibility in threshold selection. Users can choose from 23 published rainfall I-D thresholds or manually specify a custom threshold appropriate for the study area (Figure 7).

The runout and building exposure are added to the architecture as add-on modules (Figure 8). The runout model enhances hazard assessment by delineating potential debris flow impact zones from pixels exceeding a minimum warning level (≥3). Using a reach angle of 11° (default, but customizable) and a maximum search radius of 3000 m (customizable), the model simulates downslope propagation of debris flows. The framework can generate both current and forecasted runout extents (e.g., 6, 12, and 24-hour forecasts), which can be overlaid with building footprints to assess exposure.

https://doi.org/10.5194/egusphere-2026-4588
Preprint. Discussion started: 21 August 2026

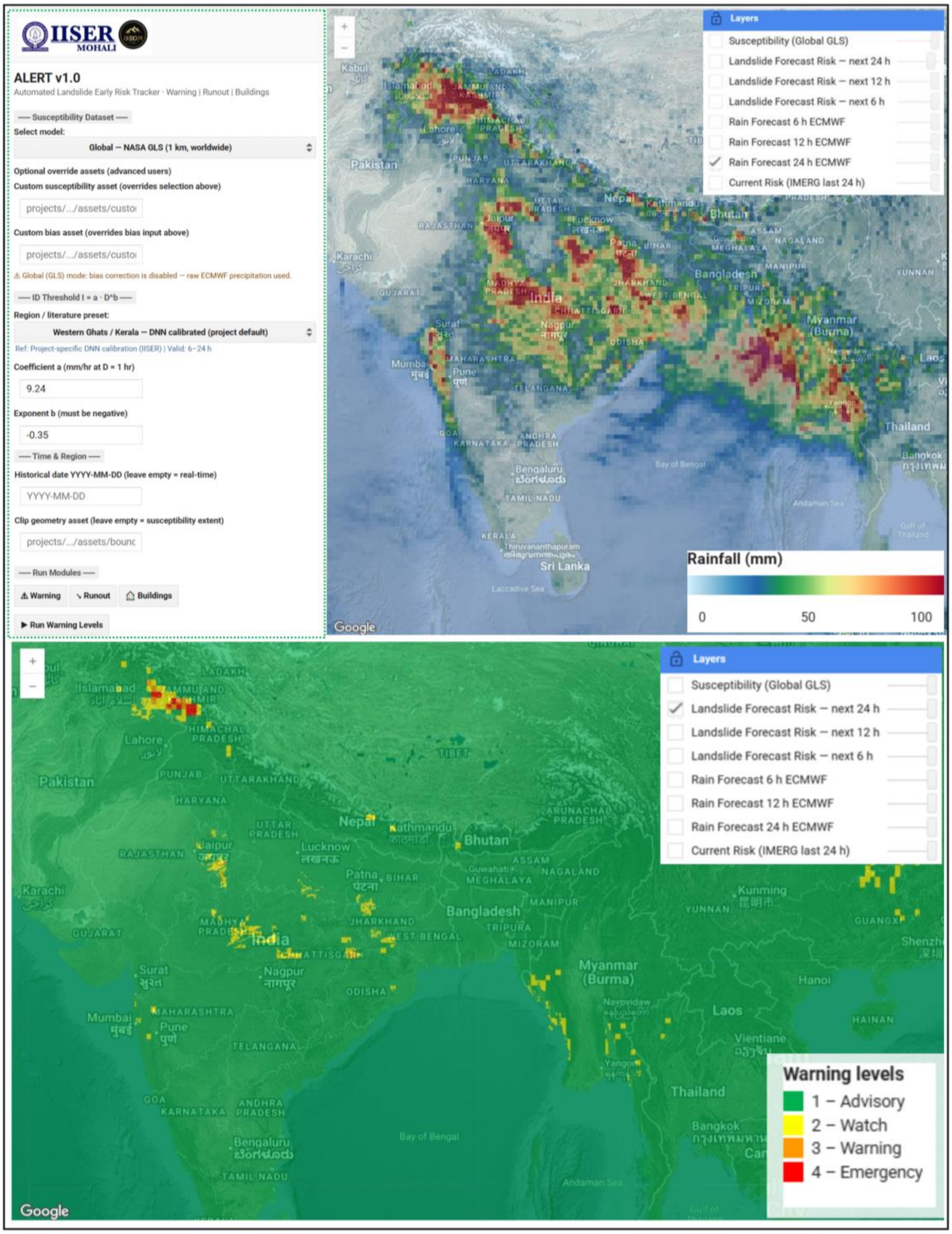

Figure 6. ALERT interface showing integrated landslide hazard assessment using ECMWF forecasts and global susceptibility layer. The upper panel displays the 24 hr accumulated rain forecast from ECMWF IFS and the lower panel dispalys the real-time warning levels (Advisory, Watch, Warning, Emergency) derived from rainfall intensity–duration threshold exceedance,

https://doi.org/10.5194/egusphere-2026-4588
Preprint. Discussion started: 21 August 2026

from ECMWF 24 hr forecasted data and susceptibility layer. The control panel allows user-defined inputs for susceptibility assets, user specified threshold parameters. In the displayed scenario (Wed, 22 Jul 2026 06:46:43 GMT), the region in Western Ghats is predominantly under Advisory level, indicating rainfall conditions below triggering thresholds, whereas parts of northern India exhibits ‘warning’ conditions (Map data ©2026 Imagery © NASA).

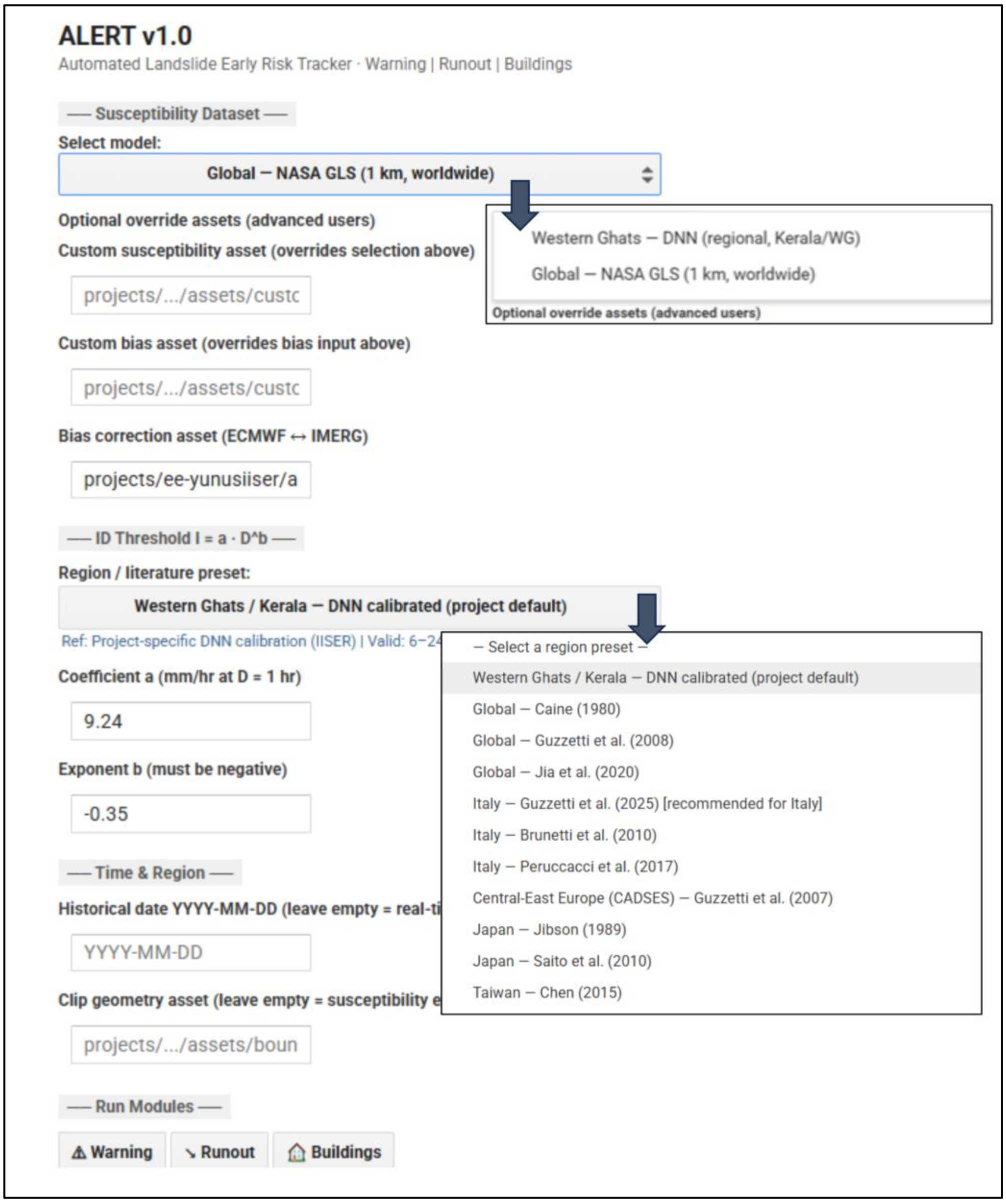

https://doi.org/10.5194/egusphere-2026-4588
Preprint. Discussion started: 21 August 2026

Figure 7. ALERT framework demonstrating its flexible configuration interface, allowing users to select from predefined rainfall intensity–duration thresholds or specify custom thresholds and susceptibility assets, thereby enabling deployment across diverse geographical and climatic environments.

The building exposure module integrates Google Open Buildings datasets with susceptibility and runout outputs to identify structures at risk (Figure 8c). Multiple layers are available, including all buildings, buildings in high susceptibility zones, and buildings intersecting predicted runout paths. In high-risk scenarios, this enables rapid identification of assets under immediate threat, supporting evacuation planning and emergency response.

We validated the I-D thresholds and the performance of the ALERT system using available landslide event dates (see Section 4.3). An example of a validation map generated by ALERT is presented in Figure 9, showing the location of the catastrophic Wayanad landslide of 29 July 2024 under Emergency conditions (red zones). Figure 8b-c shows the successful prediction of the runout zones and buildings exposed to the landslide runout.

Using the primary unique-event-day validation, ALERT correctly identified 8 of 10 landslide days, while two landslide days were missed (TP = 8; FN = 2). Four non-landslide days were incorrectly classified as warning conditions (FP = 4), whereas six were correctly classified as non-warning conditions (TN = 6). The resulting probability of detection (POD) was 0.80, with a false-alarm ratio of 0.33, precision of 0.67, specificity of 0.60, accuracy of 0.70, F1 score of 0.73, CSI of 0.57, and TSS of 0.40. These results indicate that ALERT detected a substantial proportion of observed landslide days, while also producing a measurable number of false alarms. These results should therefore be interpreted as an initial regional assessment of event discrimination.

https://doi.org/10.5194/egusphere-2026-4588
Preprint. Discussion started: 21 August 2026

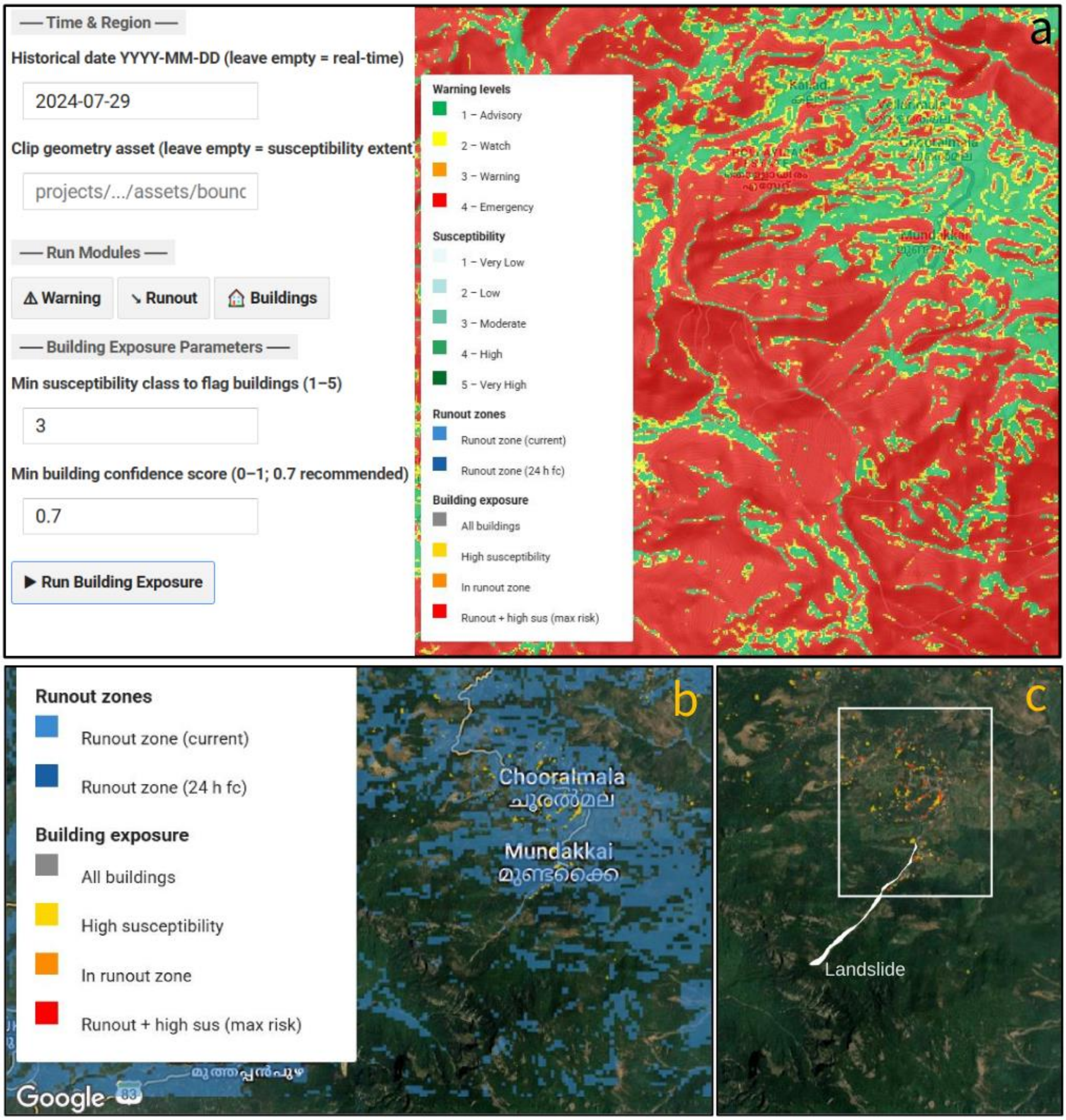

Figure 8. ALERT interface illustrating a historical simulation for 29 July 2024, one day prior to the catastrophic Wayanad landslide (Mundakkai–Chooralmala; Yunus et al., 2025). The region is predominantly classified under (a) Emergency warning
485 level (red zone), indicating that rainfall conditions exceeded the defined triggering thresholds. The application further delineates (b) active runout zones to Mundakkai and Chooralmala areas, and (c) showing building exposure to combined runout and high susceptibility in the region (Map data ©2026 Imagery © NASA).

https://doi.org/10.5194/egusphere-2026-4588
Preprint. Discussion started: 21 August 2026

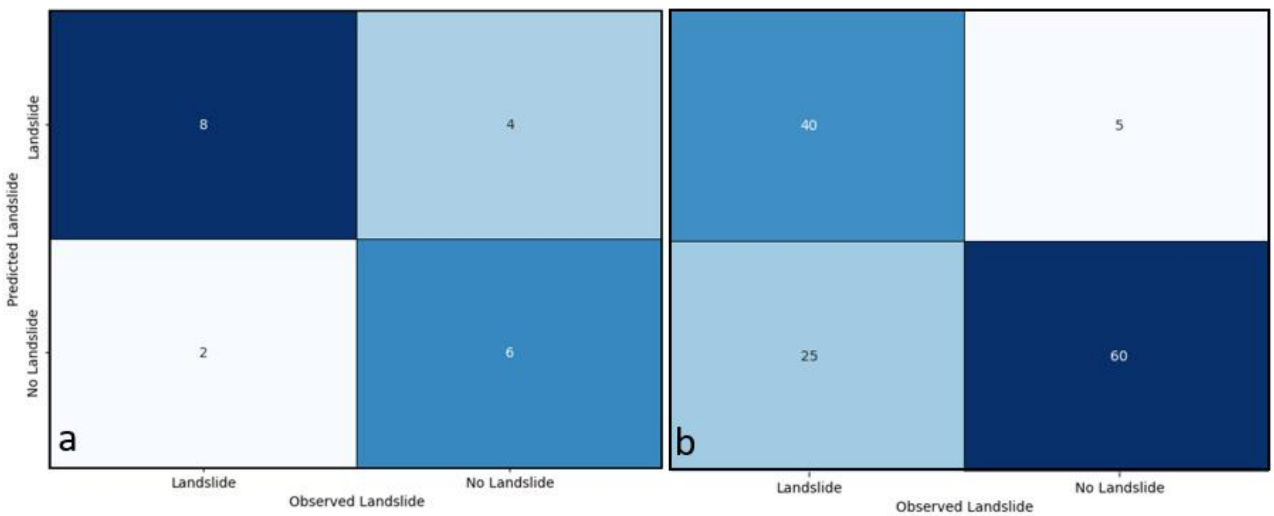

Figure 9. Confusion matrix illustrating the performance of the ALERT system under current I-D values generated for Western Ghats under (a) for unique days, and (b) for all landslide days.

6 Discussion

6.1 Strength of the ALERT system

A key advancement of the ALERT system is the unified, single-interface approach that incorporates a simplified susceptibility-cum-runout model based on the reach angle concept. While runout modelling is typically addressed separately using numerical tools such as RAMMS, FLOW-R, or DAN3D (e.g., Krishnapriya et al. 2024; Palacio et al. 2025; Rajaneesh et al. 2025), its integration within an early warning framework remains limited in the literature. The use of an empirical reach angle provides a computationally efficient method for estimating potential debris flow propagation and delineating impact zones (See Figure 8). Furthermore, the inclusion of flow channeling effects enhances realism by accounting for longer runout distances in confined drainage networks. This represents a significant step toward transitioning from hazard detection to impact-based warning systems.

Another important contribution is the integration of building exposure into the warning framework. Most existing early warning systems focus on hazard levels without explicitly linking them to elements at risk (see Figure 8c). By overlaying runout zones with building datasets, ALERT enables the identification of potentially affected assets during high-warning

https://doi.org/10.5194/egusphere-2026-4588
Preprint. Discussion started: 21 August 2026

scenarios. This capability supports actionable decision-making, such as prioritizing evacuations or allocating resources, and aligns with modern disaster risk reduction strategies that emphasize impact-based forecasting.

6.2 Limitation

Despite these advancements, certain limitations remain. The reliance on empirical I–D thresholds and reach-angle assumptions may oversimplify the complex physical processes governing landslide initiation and propagation. Moreover, the use of fixed parameters (e.g., reach angle) may not fully capture spatial variability in material properties and slope conditions. The 0.1° (≈11 km) spatial resolution of IMERG and the 0.25° resolution of ECMWF are substantially coarser than the typical scale of individual landslide-triggering rainfall cells, which may be as small as 1–2 km in convective regimes. This resolution mismatch implies that spatially averaged rainfall estimates may not capture local rainfall maxima, potentially resulting in underestimation of rainfall intensity and missed warnings for small, convectively triggered failures. The implementation of higher-resolution rainfall modelling, such as the Weather Research and Forecasting (WRF) model, together with statistical or machine-learning-based downscaling of ECMWF and IMERG precipitation, represents an important priority for future development. Such approaches could be integrated into the GEE workflow to provide higher-resolution rainfall estimates while retaining the scalability of the current framework.

6.3. Model Transferability and Scalability

The modular architecture of ALERT is explicitly designed to facilitate transferability across data-sparse, landslide-prone regions worldwide. The only region-specific components are the rainfall intensity–duration (I–D) threshold parameters (α and β) and the landslide susceptibility layer, both of which can be readily replaced or recalibrated to suit local climatic, geomorphological, and geological conditions. To enhance flexibility, ALERT includes a library of 23 published I–D thresholds spanning global, continental, national, and regional scales, while also allowing users to specify custom threshold parameters and upload their own susceptibility maps. This design enables rapid deployment of the framework in diverse geographical settings without requiring modifications to the core workflow.

The forecasting component of ALERT relies on the ECMWF IFS, which has undergone extensive global verification. According to ECMWF verification statistics (Hewson & Chevallier, 2024), forecast performance is evaluated using several complementary skill metrics, including the Continuous Ranked Probability Skill Score (CRPSS). For tropical regions, the CRPSS for 24-hour precipitation forecasts exceeds 0.1, and for Europe it exceeds 0.3, indicating that the forecasts provide measurable skill relative to climatological predictions. Although forecast uncertainty increases with lead time and in regions of complex terrain, the demonstrated skill of ECMWF IFS forecasts provides support for their use in rainfall-driven landslide forecasting within the ALERT framework. Figure 10 compares the 24-hour accumulated precipitation forecast from the ECMWF IFS, initialized on 22 July 2026, with the corresponding 24-hour accumulated rainfall observed by the Mumbai

https://doi.org/10.5194/egusphere-2026-4588
Preprint. Discussion started: 21 August 2026

Doppler Weather Radar on 23 July 2026 sourced from the India Meteorological Department (IMD). The spatial correspondence between the forecast and observed rainfall patterns provides an illustrative example of the potential utility of ECMWF IFS precipitation forecasts for operational rainfall-triggered landslide early warning within the ALERT framework.

Furthermore, ALERT incorporates an optional bias-correction module that enables users to adjust forecast rainfall using local observations or satellite-based climatologies, thereby improving forecast reliability in regions where systematic biases exist. Although the framework has been validated using the southern Western Ghats as a regional testbed, its scalability to a global context is demonstrated here by integrating a NASA-derived 1 km global landslide susceptibility layer (Stanley, and Kirschbaum, 2017) (Figure 6). For this global configuration, bias correction was not applied to ECMWF, and the threshold parameters were selected from the available threshold library (Figure 7). Consequently, the resulting warning levels may not fully reflect region-specific conditions; however, recalibration of thresholds for local hydro-climatic regimes could improve regional applicability and forecast performance. These results highlight the potential of ALERT as a globally deployable, low-infrastructure landslide early warning framework, particularly suited for regions with limited ground-based hydrometeorological observations.

7 Summary and Conclusions

This study presents ALERT (Automated Landslide Early Risk Tracker), a cloud-native, globally transferable framework and application for near-real-time rainfall-triggered landslide early warning in data-scarce regions. Unlike conventional approaches that rely solely on rainfall thresholds or susceptibility mapping, ALERT integrates satellite-based rainfall observations, numerical weather prediction, terrain susceptibility, rainfall intensity–duration (I–D) thresholds, empirical runout modelling, and exposure analysis within a unified operational framework. By coupling rainfall-triggering conditions with potential downstream impacts, ALERT extends conventional threshold-based approaches toward impact-oriented landslide early warning.

The regional IMERG-derived rainfall threshold developed for the Western Ghats ($I = 9.16D^{-0.35}$) falls within the range of published thresholds reported for humid tropical and monsoon-dominated environments. The relatively low exponent reflects the observed scaling relationship between rainfall intensity and duration and is consistent with the potential influence of prolonged monsoonal rainfall and antecedent moisture on landslide initiation, consistent with observations from other monsoon regions including Kalimpong, Bhutan, and Sri Lanka. These findings further demonstrate that although rainfall thresholds exhibit common scaling behavior, regional calibration is important for improving their operational applicability.

A major strength of ALERT is its adaptability across different geographical settings. The framework incorporates a catalogue of 23 published rainfall intensity–duration thresholds spanning global, continental, national, and regional studies, while also allowing users to define custom thresholds and susceptibility layers. Consequently, the same operational workflow can be

https://doi.org/10.5194/egusphere-2026-4588
Preprint. Discussion started: 21 August 2026

adapted to diverse climatic, geomorphological, and geological settings without modifying the core framework. Integration of NASA IMERG near-real-time precipitation with ECMWF IFS operational forecasts further enables both hindcast-based monitoring and forecast-based early warning, potentially extending warning lead times for disaster preparedness.

The key findings of this study are as follows:

- A cloud-native, globally scalable landslide early warning framework was developed that integrates satellite rainfall observations, operational weather forecasts, terrain susceptibility, debris-flow runout modelling, and building exposure analysis within a single automated workflow.
- A regional IMERG-derived rainfall threshold of $I = 9.16D^{-0.35}$ was established for the Western Ghats, providing reliable characterization of rainfall conditions associated with landslide initiation under monsoon-dominated climates.
- The ALERT framework incorporates 23 published rainfall intensity–duration thresholds, while allowing users to define custom thresholds and susceptibility layers, enabling rapid deployment across geographically diverse and data-scarce mountain regions.
- Bias-corrected ECMWF IFS precipitation forecasts, combined with IMERG observations, provide reliable rainfall forcing for operational landslide forecasting, while maintaining computational efficiency suitable for near-real-time applications.

ALERT demonstrates that satellite remote sensing and cloud computing can meaningfully close the early warning gap for data-scarce, hazard-prone regions. Future work will focus on IMERG and ECMWF downscaling, ensemble probabilistic forecasting, formal skill-score evaluation against independent event datasets, and the systematic extension of the framework to other landslide-prone mountain ranges.

https://doi.org/10.5194/egusphere-2026-4588
Preprint. Discussion started: 21 August 2026

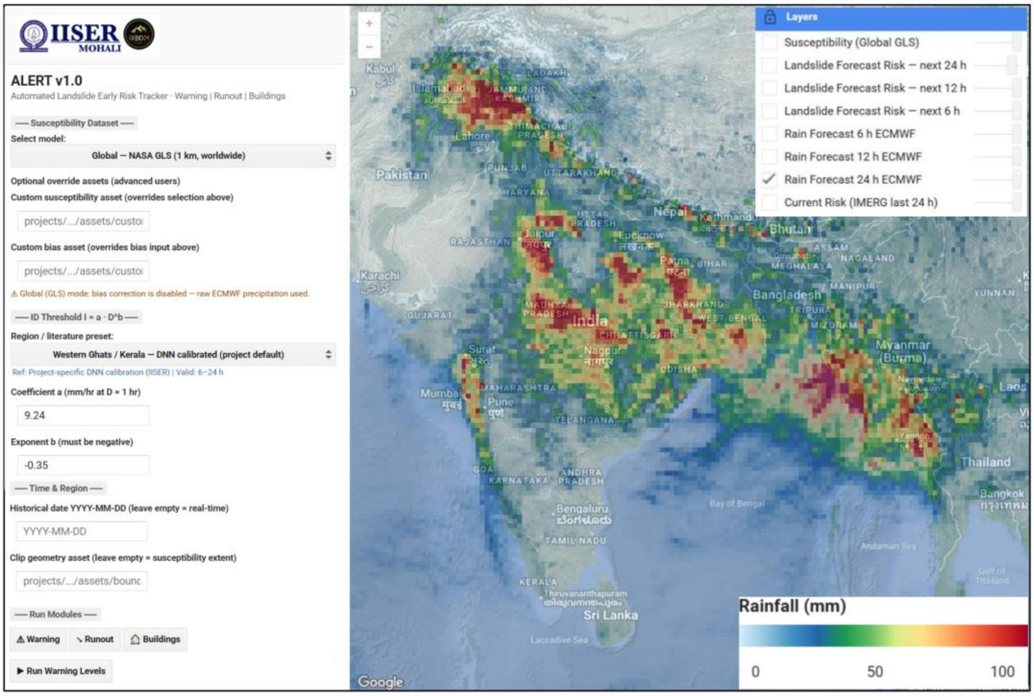

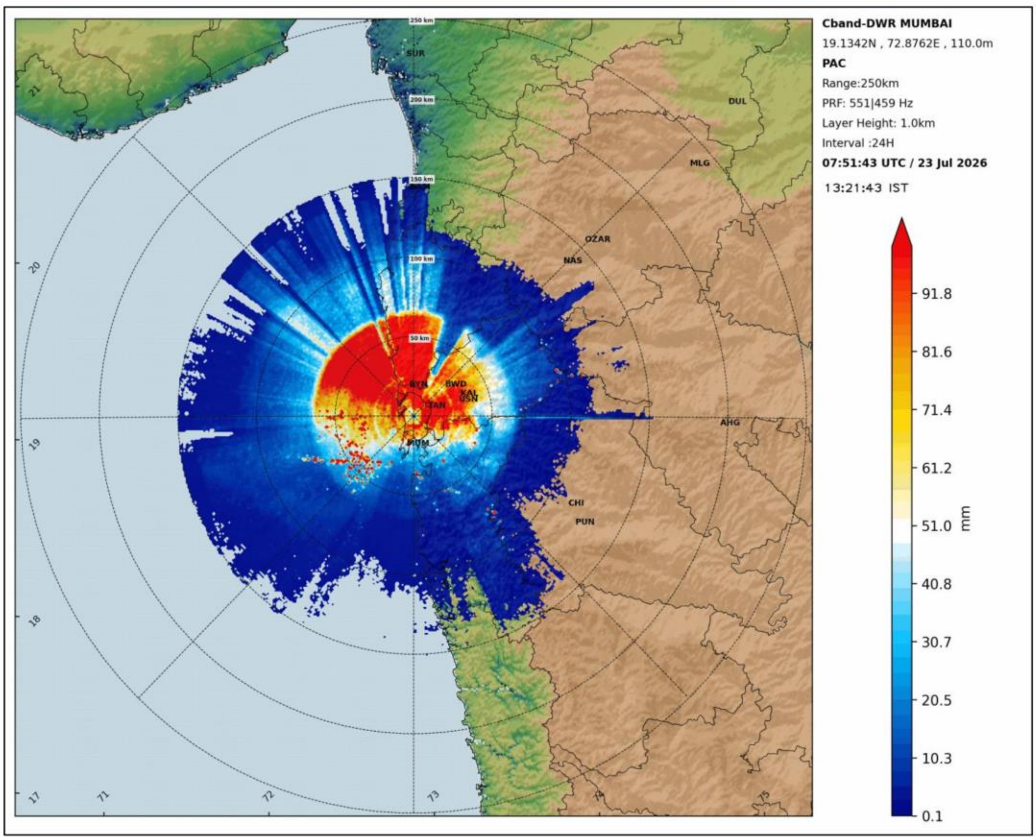

https://doi.org/10.5194/egusphere-2026-4588
Preprint. Discussion started: 21 August 2026

Figure 10. The upper panel illustrates the 24-hour accumulated precipitation forecast from the ECMWF IFS initialized on 22 July 2026 (Map data ©2026 Imagery © NASA), while the lower panel shows the corresponding 24-hour accumulated rainfall estimated from the Mumbai Doppler Weather Radar (source: IMD) on 23 July 2026.

Code and data availability

The ALERT app is available at https://ee-yunuscool.projects.earthengine.app/view/alert-app. Source code is published in the repository https://github.com/yunusapy/ALERT.

Author contributions

Conceptualisation: A.P.Y. and S.K.; Methodology: F.E.S., S.M. and A.P.Y.; Inventory compilation: S.M.; DNN modelling: A.L.A.; GEE application development: F.E.S. and A.P.Y.; Writing—original draft: A.P.Y, F.E.S., S.K., SSS.; Writing—review and editing: R.A. and A.P.Y.; Supervision: A.P.Y.; Funding acquisition: A.P.Y. S.K. and RA. All authors have read and agreed to the published version of the manuscript.

Competing interests

Authors declare no conflict of interest.

Disclaimer

Copernicus Publications remains neutral with regard to jurisdictional claims made in the text, published maps, institutional affiliations, or any other geographical representation in this paper. While Copernicus Publications makes every effort to include appropriate place names, the final responsibility lies with the authors. Views expressed in the text are those of the authors and do not necessarily reflect the views of the publisher.
Please feel free to add disclaimer text at your choice, if applicable.

Acknowledgements

The authors acknowledge IISER Mohali for the necessary research facilities.

https://doi.org/10.5194/egusphere-2026-4588
Preprint. Discussion started: 21 August 2026

Financial support

This research was funded by ISRO-DMSP grant number DMSP-ASCB/AS/2023/06 and MoE STARS grant No. STARS-2/2023-0264. The authors acknowledge IISER Mohali for the necessary research facilities.

Review statement

The review statement will be added by Copernicus Publications listing the handling editor as well as all contributing referees according to their status anonymous or identified.

References

Abraham, M. T., Pothuraju, D., and Satyam, N.: Rainfall thresholds for prediction of landslides in Idukki, India: an empirical approach, Water, 11, 2113, https://doi.org/10.3390/W11102113, 2019.

Abraham, M. T., Satyam, N., Rosi, A., Pradhan, B., and Segoni, S.: The selection of rain gauges and rainfall parameters in estimating intensity-duration thresholds for landslide occurrence: case study from Wayanad (India), Water, 12, 1000, https://doi.org/10.3390/W12041000, 2020.

Achu, A. L., Aju, C. D., Thomas, J., Raicy, M. C., Ali, P. Y., Gopinath, G., Singh, B. B., and Matthai, J.: Decoding the dynamics of July 2024 Mundakkai-Chooralmala landslide in Kerala (India): an analysis of formation mechanisms, impacts and lessons learned, Landslides, https://doi.org/10.1007/s10346-024-02454-y, 2025.

Achu, A. L., Joseph, S., Aju, C. D., and Mathai, J.: Preliminary analysis of a catastrophic landslide event on 6 August 2020 at Pettimudi, Kerala State, India, Landslides, 18, 1459–1463, https://doi.org/10.1007/s10346-020-01598-x, 2021.

Achu, A. L., Thomas, J., Aju, C. D., Vijith, H., and Gopinath, G.: Redefining landslide susceptibility under extreme rainfall events using deep learning, Geomorphology, 448, 109033, https://doi.org/10.1016/j.geomorph.2023.109033, 2024.

Ariyakumara, W. A. K. S. and Uchida, T.: Roles of different controls influencing the intensity-duration rainfall thresholds for triggering landslides: an intercomparison of published thresholds, Landslides, 1–24, https://doi.org/10.1007/s10346-025-02674-w, 2026.

Barthélemy, S., Bernardie, S., and Grandjean, G.: Assessing rainfall threshold for shallow landslides triggering: a case study in the Alpes Maritimes region, France, Nat. Hazards, 121, 4023–4049, 2025.

Beljaars, A., Garcia-Mendez, A., Ghelli, A., Trigo, I., Viterbo, P., and Zeng, X.: Biases in the ECMWF model, in: Proc. ECMWF/EUMETSAT Workshop on Bias Estimation in Data Assimilation, Reading, UK, 29–39, 2005.

Brunetti, M. T., Peruccacci, S., Rossi, M., Luciani, S., Valigi, D., and Guzzetti, F.: Rainfall thresholds for the possible occurrence of landslides in Italy, Nat. Hazards Earth Syst. Sci., 10, 447–458, https://doi.org/10.5194/nhess-10-447-2010, 2010.

Caine, N.: The rainfall intensity-duration control of shallow landslides and debris flows, Geogr. Ann. A, 62, 23–27, https://doi.org/10.2307/520449, 1980.

Chang, K., Merghadi, A., Ali, P. Y., Pham, B. T., and Dou, J.: Evaluating scale effects of topographic variables in landslide susceptibility models using GIS-based machine learning techniques, Sci. Rep., 9, 48773, https://doi.org/10.1038/s41598-019-48773-2, 2019.

Devoli, G., Tiranti, D., Cremonini, R., Sund, M., and Boje, S.: Comparison of landslide forecasting services in Piedmont (Italy) and Norway, illustrated by events in late spring 2013, Nat. Hazards Earth Syst. Sci., 18, 1351–1372, 2018.

Dixit, S., Siva Subramanian, S., Srivastava, P., Yunus, A. P., Martha, T. R., and Sen, S.: Numerical-model-derived intensity-duration thresholds for early warning of rainfall-induced debris flows in a Himalayan catchment, Nat. Hazards Earth Syst. Sci., 24, 465–480, 2024.

Dou, J., Ali, P. Y., Bui, D. T., Merghadi, A., Sahana, M., Zhu, Z., Chen, C. W., Han, Z., and Pham, B. T.: Improved landslide assessment using support vector machine with bagging, boosting, and stacking ensemble machine learning framework in a mountainous watershed, Japan, Landslides, 17, 617–631, https://doi.org/10.1007/s10346-019-01286-5, 2020.

Farahmand, A. and AghaKouchak, A.: A satellite-based global landslide model, Nat. Hazards Earth Syst. Sci., 13, 1259–1267, 2013.

Fidan, S., Görüm, T., Akbaş, A., Ekberzade, B., and Ozturk, U.: Wealth and land-cover change govern landslide fatalities on world's mountains, Sci. Adv., 12, 2739, https://doi.org/10.1126/SCIADV.AEC2739, 2026.

Froude, M. J. and Petley, D. N.: Global fatal landslide occurrence from 2004 to 2016, Nat. Hazards Earth Syst. Sci., 18, 2161–2181, https://doi.org/10.5194/nhess-18-2161-2018, 2018.

Gonzalez, F. C. G., Cavacanti, M. d. C. R., Ribeiro, W. N., Mendonça, M. B. d., and Haddad, A. N.: A systematic review on rainfall thresholds for landslides occurrence, Heliyon, 10, e23247, https://doi.org/10.1016/j.heliyon.2023.e23247, 2024.

Guzzetti, F., Peruccacci, S., Rossi, M., and Stark, C. P.: Rainfall thresholds for the initiation of landslides in central and southern Europe, Meteorol. Atmos. Phys., 98, 239–267, https://doi.org/10.1007/s00703-007-0262-7, 2007.

Guzzetti, F., Melillo, M., and Mondini, A. C.: Landslide predictions through combined rainfall threshold models, Landslides, 22, 137–147, 2025.

Harilal, G. T., Madhu, D., Ramesh, M. V., and Pullarkatt, D.: Towards establishing rainfall thresholds for a real-time landslide early warning system in Sikkim, India, Landslides, 16, 2395–2408, 2019.

He, S., Wang, J., and Liu, S.: Rainfall event-duration thresholds for landslide occurrences in China, Water, 12, 494, 2020.

Hewson, T. and Chevallier, M.: Use and verification of ECMWF products in member and co-operating states (2016), European Centre for Medium-Range Weather Forecasts, https://doi.org/10.21957/734d5d4d39, 2017.

Hong, Y., Adler, R., and Huffman, G.: Evaluation of the potential of NASA multi-satellite precipitation analysis in global landslide hazard assessment, Geophys. Res. Lett., 33, L21402, 2006.

https://doi.org/10.5194/egusphere-2026-4588
Preprint. Discussion started: 21 August 2026

Huffman, G. J., Stocker, E. F., Bolvin, D. T., Nelkin, E. J., and Tan, J.: GPM IMERG final precipitation L3 half hourly 0.1 degree × 0.1 degree V06, Greenbelt, MD, Goddard Earth Sciences Data and Information Services Center (GES DISC) [data set], https://doi.org/10.5067/GPM/IMERG/3B-HH/07, 2019.

Islam, S., Thanveer, J., Yunus, A. P., Beetan, Y., Umrikar, B., Arya, D. S., and Siva Subramanian, S.: Impact of antecedent rainfall and soil saturation on widespread debris flows in the northern Western Ghats during the 2021 extreme rainfall, Bull. Eng. Geol. Environ., 84, 360, https://doi.org/10.1007/s10064-025-04383-z, 2025.

Jia, G., Tang, Q., and Xu, X.: Evaluating the performances of satellite-based rainfall data for global rainfall-induced landslide warnings, Landslides, 17, 283–299, 2020.

Jibson, R. W.: Debris flows in southern Puerto Rico, in: Debris Flow Hazards and Related Phenomena, Geological Society of America Special Paper, 236, 29–55, 1989.

Jiang, W., Chen, G., Meng, X., Jin, J., Zhao, Y., Lin, L., Li, Y., and Zhang, Y.: Probabilistic rainfall threshold of landslides in data-scarce mountainous areas: a case study of the Bailong River Basin, China, CATENA, 213, 106190, https://doi.org/10.1016/j.catena.2022.106190, 2022.

Jordanova, G., Gariano, S. L., Melillo, M., Peruccacci, S., Brunetti, M. T., and Jemec Auflič, M.: Determination of empirical rainfall thresholds for shallow landslides in Slovenia using an automatic tool, Water, 12, 1449, 2020.

Kaushal, S., Thanveer, J., Islam, S. M. U., Negi, A., Dhanshyan, A., Beetan, Y., Siva Subramanian, S., Sajinkumar, K. S., and Ali, P. Y.: Unveiling the amplifying impact: anthropogenic activities and the two-fold surge in landslides in the Lesser Himalayas, CATENA, 250, 108771, https://doi.org/10.1016/j.catena.2025.108771, 2025.

Khan, S., Kirschbaum, D. B., and Stanley, T.: Investigating the potential of a global precipitation forecast to inform landslide prediction, Weather Clim. Extremes, 33, 100364, 2021.

Kim, S. W., Chun, K. W., Kim, M., Catani, F., Choi, B., and Seo, J. I.: Effect of antecedent rainfall conditions and their variations on shallow landslide-triggering rainfall thresholds in South Korea, Landslides, 18, 569–582, https://doi.org/10.1007/s10346-020-01505-4, 2020.

Kirschbaum, D. and Stanley, T.: Satellite-based assessment of rainfall-triggered landslide hazard for situational awareness, Earths Future, 6, 505–523, 2018.

Kirschbaum, D. B., Stanley, T., and Simmons, J. J. N. H.: A dynamic landslide hazard assessment system for Central America and Hispaniola, Nat. Hazards Earth Syst. Sci., 15, 2257–2272, 2015.

Krishnapriya, V. K., Rajaneesh, A., Sajinkumar, K. S., Vasu, N. N., van Westen, C., Oommen, T., Yunus, A. P., Banks, V. J., and Pradeepkumar, A. P.: A rapid run-out assessment methodology for the 2024 Wayanad debris flow, npj Nat. Hazards, 1, 41, https://doi.org/10.1038/s44304-024-00044-5, 2024.

Laghari, M. M., Jagirani, S. S., Cheng, N., Irfan, M., Zardari, I. A., David, U., Akbar, Z., Zewen, Y., and Bakar, M. A.: Advances in landslide detection through Google Earth Engine: a comprehensive review, Nat. Hazards Rev., 26, 05025007, https://doi.org/10.1061/NHREFO.NHENG-2423, 2025.

https://doi.org/10.5194/egusphere-2026-4588
Preprint. Discussion started: 21 August 2026

Ma, T., Li, C., Lu, Z., and Bao, Q.: Rainfall intensity-duration thresholds for the initiation of landslides in Zhejiang Province, China, Geomorphology, 245, 193–206, 2015.

Mandal, P. and Sarkar, S.: Estimation of rainfall threshold for the early warning of shallow landslides along National Highway-10 in Darjeeling Himalayas, Nat. Hazards, 105, 2455–2480, https://doi.org/10.1007/s11069-020-04407-9, 2020.

Maturidi, A. M. A. M., Kasim, N., Taib, K. A., and Azahar, W. N. A. W.: Rainfall-induced landslide thresholds development by considering different rainfall parameters: a review, J. Ecol. Eng., 22, 85–97, 2021.

Merghadi, A., Ali, P. Y., Dou, J., Whiteley, J. S., Pham, B. T., Bui, D. T., Avtar, R., and Abderrahmane, B.: Machine learning methods for landslide susceptibility studies: a comparative overview of algorithm performance, Earth-Sci. Rev., 207, 103225, https://doi.org/10.1016/j.earscirev.2020.103225, 2020.

Mohan, S., Rajaneesh, A., Krishnapriya, V. K., Sajinkumar, K. S., van Westen, C., Vasu, N. N., Yunus, A. P., Hao, L., Vishnu, C. L., and Ajin, R. S.: Slope Instability Predictor-Kerala (SLIP-K): a mobile/web application for landslide hazard prediction in Idukki, India, Earth Syst. Environ., 10, 3657–3679, 2026.

Nadim, F., Kjekstad, O., Peduzzi, P., Herold, C., and Jaedicke, C.: Global landslide and avalanche hotspots, Landslides, 3, 159–173, 2006.

Nawagamuwa, U. P. and Perera, L. P.: Recommending rainfall thresholds for landslides in Sri Lanka, in: Advancing Culture of Living with Landslides, 267–272, 2017.

Niyokwiringirwa, P., Lombardo, L., Dewitte, O., Deijns, A. A. J., Wang, N., van Westen, C. J., and Tanyas, H.: Event-based rainfall-induced landslide inventories and rainfall thresholds for Malawi, Landslides, 21, 1403–1424, https://doi.org/10.1007/s10346-023-02203-7, 2024.

Oorthuis, R., Hürlimann, M., Vaunat, J., Moya, J., and Lloret, A.: Monitoring the role of soil hydrologic conditions and rainfall for the triggering of torrential flows in the Rebaixader catchment (Central Pyrenees, Spain), Landslides, 20, 249–269, 2023.

Osanai, N., Shimizu, T., Kuramoto, K., Kojima, S., and Noro, T.: Japanese early-warning for debris flows and slope failures using rainfall indices with radial basis function network, Landslides, 7, 325–338, https://doi.org/10.1007/s10346-010-0229-5, 2010.

Palacio, J., Aristizábal, E., Mergili, M., and Echeverrí, O.: Exploring best-fit parameters for propagation modeling of shallow landslides, using Flow-R, J. S. Am. Earth Sci., 166, 105739, https://doi.org/10.1016/j.jsames.2025.105739, 2025.

Peruccacci, S., Brunetti, M. T., Gariano, S. L., Melillo, M., Rossi, M., and Guzzetti, F.: Rainfall thresholds for possible landslide occurrence in Italy, Geomorphology, 290, 39–57, https://doi.org/10.1016/j.geomorph.2017.03.031, 2017.

Peruccacci, S., Brunetti, M. T., Luciani, S., Vennari, C., and Guzzetti, F.: Lithological and seasonal control on rainfall thresholds for the possible initiation of landslides in central Italy, Geomorphology, 139–140, 79–90, https://doi.org/10.1016/j.geomorph.2011.10.005, 2012.

Piciullo, L., Gariano, S. L., Melillo, M., Brunetti, M. T., Peruccacci, S., Guzzetti, F., and Calvello, M.: Definition and performance of a threshold-based regional early warning model for rainfall-induced landslides, Landslides, 14, 995–1008, 2017.

Rajaneesh, A., Krishnapriya, V. K., Sajinkumar, K. S., Vasu, N. N., van Westen, C., Oommen, T., Yunus, A. P., Banks, V. J., and Pradeepkumar, A. P.: Predicting debris flow pathways using volume-based thresholds for effective risk assessment, npj Nat. Hazards, 2, 1–?, https://doi.org/10.1038/s44304-024-00055-2, 2025.

Rickenmann, D.: Runout prediction methods, in: Debris-Flow Hazards and Related Phenomena, Springer Praxis Books, Springer, Berlin, Heidelberg, 305–324, 2005.

Saito, H., Nakayama, D., and Matsuyama, H.: Two types of rainfall conditions associated with shallow landslide initiation in Japan as revealed by normalized soil water index, SOLA, 6, 57–60, 2010.

Segoni, S., Lagomarsino, D., Fanti, R., Moretti, S., and Casagli, N.: Integration of rainfall thresholds and susceptibility maps in the Emilia Romagna (Italy) regional-scale landslide warning system, Landslides, 12, 773–785, 2015.

Shah, B., Bhat, M. S., Alam, A., Malik, U. F., Ali, N., and Sheikh, H. A.: Establishing the landslide-triggering rainfall thresholds for the Kashmir Himalaya, Nat. Hazards, 120, 1319–1341, 2024.

Sirko, W., Kashubin, S., Ritter, M., Annkah, A., Bouchareb, Y. S. E., Dauphin, Y., Keysers, D., Neumann, M., Cisse, M., and Quinn, J.: Continental-scale building detection from high resolution satellite imagery, arXiv [preprint], arXiv:2107.12283, 2021.

Stanley, T. and Kirschbaum, D. B.: A heuristic approach to global landslide susceptibility mapping, Nat. Hazards, 87, 145–164, https://doi.org/10.1007/s11069-017-2757-y, 2017.

Stanley, T. A., Kirschbaum, D. B., Benz, G., Emberson, R. A., Amatya, P. M., Medwedeff, W., and Clark, M. K.: Data-driven landslide nowcasting at the global scale, Front. Earth Sci., 9, 640043, 2021.

Wang, S., Zhang, K., Chao, L., Chen, G., Xia, Y., and Zhang, C.: Investigating the feasibility of using satellite rainfall for the integrated prediction of flood and landslide hazards over Shaanxi Province in Northwest China, Remote Sens., 15, 2457, https://doi.org/10.3390/rs15092457, 2023.

Yang, F., Fan, X., Siva Subramanian, S., Dou, X., Xiong, J., Xia, B., Yu, Z., and Xu, Q.: Catastrophic debris flows triggered by the 20 August 2019 rainfall, a decade since the Wenchuan earthquake, China, Landslides, 18, 3197–3212, https://doi.org/10.1007/s10346-021-01713-6, 2021.

Yunus, A. P., Sajinkumar, K. S., Gopinath, G., Siva Subramanian, S., Kaushal, S., Thanveer, J., Achu, A. L., Islam, S. M. U., Ishan, A., Krishnapriya, V. K., Rajaneesh, A., Dewrari, M., Dixit, S., Singh, S., Srivastava, P., Oommen, T., Vasu, N. N., Sen, S., Narayana, A. C., Ambili, V., Pradeep, G. S., and Kuriakose, S. L.: Chronicle of destruction: the Wayanad landslide of July 30, 2024, Landslides, 22, 1891–1908, https://doi.org/10.1007/s10346-025-02494-y, 2025.

Yunus, A. P., Fan, X., Siva Subramanian, S., Jie, D., and Xu, Q.: Unraveling the drivers of intensified landslide regimes in Western Ghats, India, Sci. Total Environ., 770, 145357, https://doi.org/10.1016/j.scitotenv.2021.145357, 2021.

https://doi.org/10.5194/egusphere-2026-4588
Preprint. Discussion started: 21 August 2026

Zhao, B., Dai, Q., Zhuo, L., Mao, J., Zhu, S., and Han, D.: Accounting for satellite rainfall uncertainty in rainfall-triggered landslide forecasting, Geomorphology, 398, 108051, https://doi.org/10.1016/j.geomorph.2021.108051, 2022.Abraham, Minu Treesa, Deekshith Pothuraju, and Neelima Satyam. 2019. "Rainfall Thresholds for Prediction of Landslides in Idukki, India: An Empirical Approach." Water 2019, Vol. 11, 11(10). doi:10.3390/W11102113.